Absolute instability in axisymmetric wakes: Compressible and density variation effects

P. Meliga, D. Sipp, J.-M. Chomaz

J. Fluid Mech. (2008), *vol.* 600, *pp.* 373–401.
doi:10.1017/S0022112008000499 Printed in the United Kingdom

Absolute instability in axisymmetric wakes: compressible and density variation effects

PHILIPPE MELIGA[1], DENIS SIPP[1] AND JEAN-MARC CHOMAZ[1,2]

[1]ONERA/DAFE, 8 rue des Vertugadins, 92190 Meudon, France
[2]LadHyX, CNRS-Ecole Polytechnique, 91128 Palaiseau, France

(Received 27 April 2007 and in revised form 8 January 2008)

Lesshafft & Huerre (*Phys. Fluids,* 2007; vol. 19, 024102) have recently studied the transition from convective to absolute instability in hot round jets, for which absolute instability is led by axisymmetric perturbations and enhanced when lowering the jet density. The present paper analyses similarly the counterpart problem of wake flows, and establishes that absolute instability is then led by a large-scale helical wake mode favoured when the wake is denser than the surrounding fluid. This generalizes to variable density and compressible wakes the results of Monkewitz (*J. Fluid Mech.* vol 192, 1988, p. 561). Furthermore, we show that in a particular range of density ratios, the large-scale helical wake mode can become absolutely unstable by increasing only the Mach number up to high subsonic values. This possibility of an absolute instability triggered by an increase of the Mach number is opposite to the behaviour previously described in shear flows such as plane mixing layers and axisymmetric jets. A physical interpretation based on the action of the baroclinic torque is proposed. An axisymmetric short-scale mode, similar to that observed in plane mixing layers, leads the transition in light wakes, but the corresponding configurations require large counterflow for the instability to be absolute.

These results suggest that the low-frequency oscillation present in afterbody wakes may be due to a nonlinear global mode triggered by a local absolute instability, since the azimuthal wavenumber and absolute frequency of the helical wake mode agree qualitatively with observations.

1. Introduction

Wake flows past axisymmetric bodies have been studied both experimentally and numerically in the last decades – see for instance the studies of Achenbach (1974) on spheres, of Fuchs, Mercker & Michel (1979) and Berger, Scholz & Schumm (1990) on circular disks. It has been generally acknowledged that this class of flow is dominated by an instability of the helical mode, resulting in the low-frequency shedding of large-scale coherent structures in the form of two superimposed modes of azimuthal wavenumbers $m = \pm 1$. Low Strouhal numbers of 0.2 and 0.135, characteristic of vortex-shedding phenomena, have been reported for the sphere and the disk, respectively, based on the body diameter. Kim & Durbin (1988) showed that the periodic shedding regime was intrinsic, i.e. insensitive to low levels of external acoustic excitation for forcing frequencies far enough from the natural one.

The onset of this type of self-sustained synchronized oscillations in free shear flows, such as wakes and jets, has been analysed using the local stability theory, that

computes the instability properties of a fictitious parallel flow obtained by extending to infinity the velocity profiles measured at each streamwise station. Numerous theoretical approaches have provided strong evidence that the transition from convective to local absolute instability (Briggs 1964; Bers 1975) plays a crucial role in the existence of such oscillations. The works of Koch (1985) and Monkewitz & Nguyen (1987), among others, have shown that synchronized oscillations for the two-dimensional wake are linked to the existence of a region of local absolute instability in the near wake, where the small-amplitude wave packet generated by an arbitrary perturbation propagates both in the upstream and downstream directions, and grows in time at any fixed location. Similar results have been established for sufficiently light or heated jets in the theoretical and experimental studies of Monkewitz & Sohn (1988) and Monkewitz *et al.* (1990). Striking results have also been obtained in the context of flow control. The experimental and theoretical work of Sevilla & Martínez-Bazàn (2004) shows in particular that it is possible to suppress the vortex shedding past an axisymmetric blunt-based body using a base bleed control strategy aiming at promoting the convective nature of the instability.

Recent studies have extended these analyses to the fully nonlinear regime, and have provided theoretical predictions for the onset and frequency of such synchronized oscillations in spatially developing flows. The analyses of Chomaz (1992), Couairon & Chomaz (1997) Tobias, Proctor & Knobloch (1997, 1998) and Pier, Huerre & Chomaz (2001) on model equations in semi-infinite and infinite domains have highlighted the connection between nonlinear global modes and front dynamics that characterize the propagation of a saturated instability wave into a quiescent region (Dee & Langer 1983; van Saarloos 1987, 2003), provided the streamwise variations of the baseflow are sufficiently slow (see Chomaz 2005 for a review). The main idea developed in these studies is that the nonlinear global mode is dominated by a stationary front acting like a *wavemaker*, and that its frequency and spatial structure are determined by the local linear stability properties at the upstream boundary of the region of absolute instability. These conclusions apply under the assumption that the front velocity is linearly selected, i.e. the front is pulled under the action of linear mechanisms at work in the upstream tail (van Saarloos 2003). In that case, if the flow displays convectively unstable inlet conditions, so that absolute instability arises only beyond a specific downstream station x^{ca}, then the associated spatial structure consists of a steep front pinned at this position of marginal absolute instability. The front then separates an upstream region of vanishing amplitude, where perturbations decay exponentially, from the finite-amplitude downstream tail, made of a saturated wavetrain. The global frequency is then given by the linear absolute frequency ω_r^{0ca} at this transition station x^{ca}, and the spatial growth rate upstream of the front is given by the absolute wavenumber $-k_i^{0ca}$. In the case where the flow displays an absolutely unstable inlet conditions, the front is pinned against the body, where the perturbation amplitude is forced to be zero. The same global frequency selection criterion applies at the threshold of global instability, i.e. the global frequency is given by ω_r^{0inlet}. Above the global instability threshold, the criterion provides only a leading-order prediction of the global frequency (Couairon & Chomaz 1999).

These theoretical predictions, rigorously derived only for these model equations, have been shown to apply also to real flow configurations. In the case of a two-dimensional *synthetic* wake – i.e. with no solid boundaries and no recirculation –, Pier & Huerre (2001) demonstrated that absolute instability arises beyond a specific downstream position x^{ca}. They also found that the upstream front of the vortex street was located at x^{ca} and that the frequency of the von Kármán vortex street, as observed

in direct numerical simulations, matches the absolute frequency ω_0^{ca} within 2 %. In the naturally developing wake behind a circular cylinder, despite the fact that the slow streamwise variation hypothesis is not valid in the separated region, Pier (2002) has shown that the same frequency criterion provides a 10 % accurate prediction over the range of Reynolds numbers $100 \leqslant Re \leqslant 180$. Similar work has been carried out by Gallaire & Chomaz (2003) in the case of the double helix mode arising in swirling jets, by Lesshafft *et al.* (2006) in the case of hot round jets and by Gallaire *et al.* (2006) in the case of spiral vortex breakdown. Lesshafft *et al.* (2006) also considered the case of an absolutely unstable inlet condition, where the frequency selection criterion is valid in the vicinity of the global instability threshold. These studies show that, as for model equations, the global oscillations observed in these flows may be interpreted as a nonlinear global mode driven by a pulled front located at the upstream station of marginal absolute instability x^{ca} or at the inlet when the flow is absolutely unstable there, the global frequency being approximated well by the absolute frequency at the front location, at least close to the global instability threshold.

Following this line of thought, we view unsteadiness in the wake of axisymmetric bodies as the manifestation of such a nonlinear global mode induced by a region of absolute instability. Therefore, only critical parameters at the transition between convective and absolute instability matter in predicting the existence and the frequency of such unstable modes. Consistently with experimental observations, the inviscid analysis of Monkewitz (1988) has already shown that in the incompressible homogeneous limit, such axisymmetric wakes can sustain a helical absolute instability of azimuthal wavenumber $m = 1$. However, many applications, such as afterbody flows, require us to consider the effect of compressibility and density variations, as in the experimental studies of Flodrops & Desse (1985) and Depres, Reijasse & Dussauge (2004). The present study aims at generalizing the study of Monkewitz to non-homogeneous compressible wakes, and at providing a complete characterization of the convective/absolute transition of axisymmetric wake models and eventually to predict the onset and frequency of self-sustained oscillations in more complex flow configurations. In particular, physical interpretations are given in terms of a baroclinic factor, that extends to non-axisymmetric perturbations and compressible flow the effect of the baroclinic torque on the instability, discussed by Lesshafft *et al.* (2006) and Nichols, Schmid & Riley (2007) in the case of jets. The paper is organized as follows: the problem formulation for the base flow and its disturbances is given in § 2.1. Section 2.2 presents the numerical procedure used to determine the linear instability properties of the base flow. In § 3, the different instability modes of interest are identified through an investigation of the linear impulse response that highlights the wake/jet dichotomy and the azimuthal wavenumber selection. In §§ 4.1 to 4.3, we provide a characterization of the convective/absolute transition in terms of control parameter ranges (Mach number, steepness parameter, velocity and density ratios), frequency and wavenumber.

2. Theoretical framework

2.1. *Parallel base flow and disturbances*

We consider a non-homogeneous compressible ideal gas with constant specific heat c_p, thermal conductivity κ, and dynamic viscosity μ, related by a unit Prandtl number. All equations are formulated in cylindrical coordinates (r, θ, z). We use the upstream quantities ρ_∞, T_∞ and P_∞ as density, temperature and pressure scales respectively. The

fluid motion is governed by the compressible Navier–Stokes equations, written as

$$D_t\rho + \rho\nabla\cdot\boldsymbol{u} = 0, \tag{2.1}$$

$$\rho D_t\boldsymbol{u} = -\frac{1}{\gamma M_\infty^2}\nabla p + \frac{1}{Re_\infty}\Delta\boldsymbol{u}, \tag{2.2}$$

$$\rho D_t T = -p\nabla\cdot\boldsymbol{u} + \gamma(\gamma-1)\frac{M_\infty^2}{Re_\infty}\left(-\tfrac{2}{3}\nabla\cdot\boldsymbol{u}^2 + 2\boldsymbol{d}:\boldsymbol{d}\right) + \frac{\gamma}{PrRe}\Delta T, \tag{2.3}$$

where D_t is the material derivative, $\boldsymbol{d}$ is the strain tensor given by

$$\boldsymbol{d} = \tfrac{1}{2}\left(\nabla\boldsymbol{u} + \nabla\boldsymbol{u}^T\right) \tag{2.4}$$

and the Reynolds, Mach and Prandtl numbers are defined as

$$Re_\infty = \frac{\rho_\infty R W_\infty}{\mu}, \qquad M_\infty = \frac{W_\infty}{\sqrt{\gamma R_g T_\infty}}, \qquad Pr = \frac{\mu c_p}{\kappa}, \tag{2.5}$$

with R_g and γ the ideal gas constant and the ratio of specific heats.

The unperturbed wake is assumed to be steady, axisymmetric and uniform in the axial direction. This holds under the assumption that the instability wavelength is short compared to the viscous diffusion spatial scale. The base flow is therefore chosen as an inviscid solution of (2.1)–(2.3). An analytical expression of the velocity profile is taken from the studies of Monkewitz & Sohn (1988) and Monkewitz (1988). In dimensional variables, indicated by an asterisk, the base flow under consideration reads:

$$W_b^*(r^*) = W_\infty + (W_c - W_\infty)F(r^*), \tag{2.6}$$

where $F(r^*)$ is the distribution

$$F(r^*) = \frac{1}{1 + \left(2^{(r^*/R)^2} - 1\right)^N}. \tag{2.7}$$

In (2.6), subscripts c and ∞ refer, respectively, to the centreline and free-stream velocities. In (2.7), R is the wake radius R defined as $W_b^*(R) = W_m$ where W_m is the mean velocity $W_m = (W_c + W_\infty)/2$. Using the mean velocity W_m as velocity scale and the wake radius R as length scale, we introduce the velocity ratio $\Lambda = (W_c - W_\infty)/(W_c + W_\infty)$. In non-dimensional variables, the base flow reads

$$W_b(r) = 1 - \Lambda + \frac{2\Lambda}{1 + (2^{r^2} - 1)^N}. \tag{2.8}$$

In the context of wakes, Λ varies in the range $-\infty < \Lambda < 0$, with $\Lambda = -1$ in the particular case of a wake with zero centreline velocity. The centreline and free streams are coflowing for $-1 < \Lambda < 0$ and counterflowing for $\Lambda < -1$. Positive values of Λ correspond to jet velocity profiles. Figure 1 shows typical wake and jet profiles that are symmetric with respect to the unity velocity, i.e. $W_b(\Lambda, r) = 2 - W_b(-\Lambda, r)$. The thickness of the shear layer is characterized by the steepness parameter D/θ, where D is the wake diameter $D = 2R$ and θ is the momentum thickness defined in the homogeneous limit as

$$(W_\infty - W_c)^2\theta = \int_0^\infty (W_b(r) - W_c)(W_\infty - W_b(r))\,\mathrm{d}r. \tag{2.9}$$

Considering variations of θ relative to a fixed diameter D, this parameter allows for continuous variation between the top-hat wake bounded by a cylindrical vortex

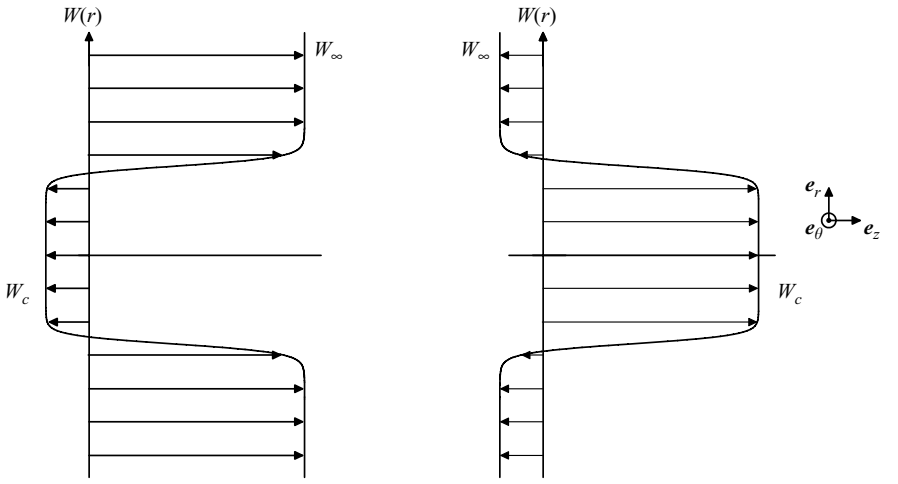

FIGURE 1. Typical velocity wake profile, and corresponding jet profile symmetric with respect to the unity velocity.

sheet obtained for $N \to \infty$ ($D/\theta \to \infty$), and the Gaussian profile obtained for $N = 1$ ($D/\theta = 6.5$). For $N < 1$, this family of profiles is not appropriate, as the second-order derivative of the velocity profile is singular at $r = 0$. The corresponding range of steepness parameters accessible through (2.6)–(2.7) is therefore $6.5 \leqslant D/\theta < \infty$.

In the absence of body forces, the pressure P_b is uniform throughout the flow. For a fixed ratio of centreline to free-stream density $S = \rho_c/\rho_\infty$ ($S > 1$ for cold heavy wakes and $S < 1$ for hot light wakes), the energy equation for the base flow is replaced by the Crocco–Busemann relation (Schlichting 1978), obtained from the three-dimensional steady boundary-layer equations, and modelling a heat transport across the shear layer similar to the momentum transport. The temperature field is given by

$$T_b(r) = 1 + \left(\frac{1}{S} - 1\right) F(r) - \frac{(\gamma - 1)M_\infty^2}{2} \left(\frac{2\Lambda}{1 - \Lambda}\right)^2 F(r)(F(r) - 1) \tag{2.10}$$

and the density is obtained from the ideal gas relation as

$$\rho_b(r) = T_b(r)^{-1}. \tag{2.11}$$

In the framework of the linear stability theory, all flow field quantities are decomposed into base flow and infinitesimal disturbances (ρ', u', v', w', t', p') where u', v', w' are the radial, azimuthal and axial components of the velocity perturbation. Disturbances are chosen in the usual normal mode form

$$\phi(r, \theta, z, t) = \phi_b(r) + \epsilon\left(\phi'(r) \mathrm{e}^{\mathrm{i}(kz + m\theta - \omega t)} + \text{ c.c.}\right) \tag{2.12}$$

where c.c. denotes the complex conjugate and ϕ' stands for any disturbance quantity. The term $k = k_r + \mathrm{i}k_i$ is the complex axial wavenumber, $\omega = \omega_r + \mathrm{i}\omega_i$ is the complex pulsation, ω_i and $-k_i$ being, respectively, the temporal and spatial growth rates, and m is the integer azimuthal wavenumber. Substitution of (2.12) into the governing equations (2.1)–(2.3) linearized about the base flow and elimination of the pressure disturbances p' lead to a generalized eigenvalue problem for either k or ω, whose equations are given in Appendix A. For all calculations, a complete set of eigenvalues and associated eigenfunctions is obtained for a Reynolds number $Re_\infty = 2000$, using a spectral Chebyshev–Gauss collocation method.

2.2. Numerical method

A mode of zero group velocity $\partial\omega/\partial k = 0$ is associated with a saddle point k^0 and a branch point $\omega^0 = \omega(k^0)$ for the complex pulsation $\omega(k)$. The saddle point k^0 must be *causal* and be formed by the pinching of an upstream and a downstream propagating branch, i.e. the spatial branches issuing from the saddle point must separate into the upper and lower half of the complex k-plane when $\omega_i \geqslant \omega_{i,max}$, where $\omega_{i,max}$ is the maximum temporal growth rate, the largest ω_i over all temporal waves with $k \in \mathbb{R}$. A mode of non-zero group velocity $\partial\omega/\partial k = v_g$ is associated with a wavenumber k^v and a pulsation $\omega^v = \omega(k^v)$, corresponding to a saddle point $\tilde{k}^0$ and a branch point $\tilde{\omega}^0 = \tilde{\omega}(\tilde{k}^0)$ in the Galilean frame travelling at the velocity v_g for the accordingly modified velocity scale and resulting dimensionless parameters, obtained as

$$\tilde{\omega}^0 = \omega^v - v_g k^v, \tag{2.13a}$$

$$\tilde{k}^0 = k^v. \tag{2.13b}$$

In the present study, modes of zero group velocity are searched by an iterative procedure: owing to the saddle point singularity in the complex k-plane, $\omega(k)$ admits a quadratic Taylor expansion around k^0. The numerical procedure used follows that of Deissler (1987): saddle points k^0 are computed by fitting a generic quadratic expression of the form

$$\omega(k) = \omega^0 + l(k - k^0)^2 \tag{2.14}$$

on the eigenvalues $\omega(k^{(i)})$ obtained for three wavenumbers $k^{(i)}$ close to an initial guess value of k^0. All constants k^0, ω^0 and l are computed and three new wavenumbers are chosen closer to the extrapolated value of k^0. The procedure is repeated until both k^0 and ω^0 become stationary within the desired tolerance (four significant digits in the present study). Note that the discrimination between pinching points and physically impermissible k^-/k^- saddle points requires the computation of the spatial branches. For modes of group velocity v_g, k^v and ω^v are obtained similarly by using a quadratic expression of the form

$$\omega(k) = \omega^v + v_g(k - k^v) + l(k - k^v)^2 . \tag{2.15}$$

This method was found to provide results matching the associated saddle point in the co-moving frame $(\tilde{r}^*, \tilde{z}^*) = (r^*, z^* - v_g^* t^*)$.

In the laboratory frame, the asymptotic impulse response of the flow at large times is proportional to the quantity $\exp(\mathrm{i}(k^0 z + m\theta - \omega^0 t))$ – see Huerre & Monkewitz (1985). Therefore, only the k^+/k^- pinching point of highest absolute growth rate is taken into account in this study, as this mode will dominate in the long time limit. The base flow is then classified as absolutely unstable if a mode of zero group velocity has a positive absolute growth rate ω_i^0 and fulfils the pinching requirements. In the following, we use the Strouhal number St built up from ω_r^0, W_∞ and D, and the absolute wavelength λ^0 built up from k_r^0 and D, defined by

$$St = \frac{\omega_r^0 D}{2\pi W_\infty}, \qquad \lambda^0 = \frac{2\pi}{k_r^0 D} . \tag{2.16}$$

Similarly, for a non-zero group velocity, we use the wavelength λ^v built up from k_r^v and D.

3. Linear impulse response of an incompressible wake

In the linear stability theory, an arbitrary perturbation generates a small-amplitude wave packet composed, for any particular azimuthal wavenumber, of a continuous set of spatio-temporal modes, each mode propagating with its own specific group velocity. In this section, the linear impulse response of an axisymmetric wake is investigated in the zero-Mach-number limit as a convenient way to identify the spatio-temporal modes of interest. All results are provided in terms of the spatio-temporal growth rate $\sigma = \omega_i^v - v_g k_i^v$. Note that the linear impulse response for a wake flow represents also the impulse response of the jet flow with $\Lambda^{jet} = -\Lambda^{wake}$ (see figure 1), if a symmetry with respect to $v_g = 1$ is applied, i.e. $\sigma(v_g^{jet}) = \sigma(2 - v_g^{wake})$. This symmetry is of particular importance when the absolute–convective transition is of interest, as the trailing edge and the leading edge of the wave packet exchange roles. For clarity, the properties of the trailing and leading edges are always discussed for a wake wave packet propagating in a wake flow, i.e. the trailing edge is located at the 'wake side' of the wave packet, and the leading edge at 'the jet side' of the wave packet. A wake of particular Λ will then be absolutely unstable if the *trailing* edge of the impulse response travels with a velocity $v_g < 0$, whereas the jet counterpart will be absolutely unstable if the *leading* edge travels with a velocity $v_g > 2$. This section extends to the 'wake side' of the wave packet the study of Lesshafft & Huerre (2007), where the impulse response is computed and discussed only for the 'jet side'.

3.1. *Helical wave packet, $m = 1$*

We choose a profile characterized by a velocity ratio $\Lambda = -1.2$ (corresponding to a centreline counterflow of 9% of the free-stream velocity) and a steepness parameter $D/\theta = 60$ to illustrate the physics of the impulse response. Figure 2(*a*) shows the spatio-temporal growth rate σ of the helical modes ($m = 1$) as a function of the group velocity v_g (thick line).

At the trailing edge of the wave packet, the spatio-temporal growth rate distribution exhibits an angular point for $v_g = 0.080$ that divides the wave packet into two domains, corresponding to two distinct modes. Modes dominating at low group velocities $v_g \leqslant 0.080$ correspond to absolute instability modes which trigger the vortex-shedding phenomenon in homogeneous wakes (Monkewitz 1988). These modes will be referred to as *wake* modes. Modes dominating at higher group velocities $v_g \geqslant 0.080$ continually extend to the other side of the wave packet. These modes, that will be referred to as *shear-layer* modes, are the equivalent for $m = 1$ of the short-scale modes that have been identified in hot jets by Jendoubi & Strykowski (1994) for axisymmetric disturbances ($m = 0$).

This distinction between wake and shear-layer modes is confirmed by figure 3(*a*), where the radial velocity eigenfunctions u' of each mode are presented, respectively, for $v_g = 0$ (wake mode) and $v_g = 0.15$ (shear-layer mode). All velocity magnitudes have been normalized with respect to the maximum radial velocity perturbation. For both modes, a non-zero radial velocity component of the disturbance energy is allowed in the centreline region by the boundary conditions that apply at $r = 0$ for $m = 1$. As expected for the shear-layer mode, the perturbation is concentrated in the shear-layer region, decays rapidly at large cross-stream distances and when approaching the centreline. For the wake mode, the perturbation also peaks in the shear region, but maintains a significant level at larger cross-stream distances. The large value of the perturbations at $r = 0$ indicates that the shear layer can no longer be considered as isolated, but interacts strongly with the boundary condition at the centreline. The wavelength λ^v at the angular point close to the trailing edge of the

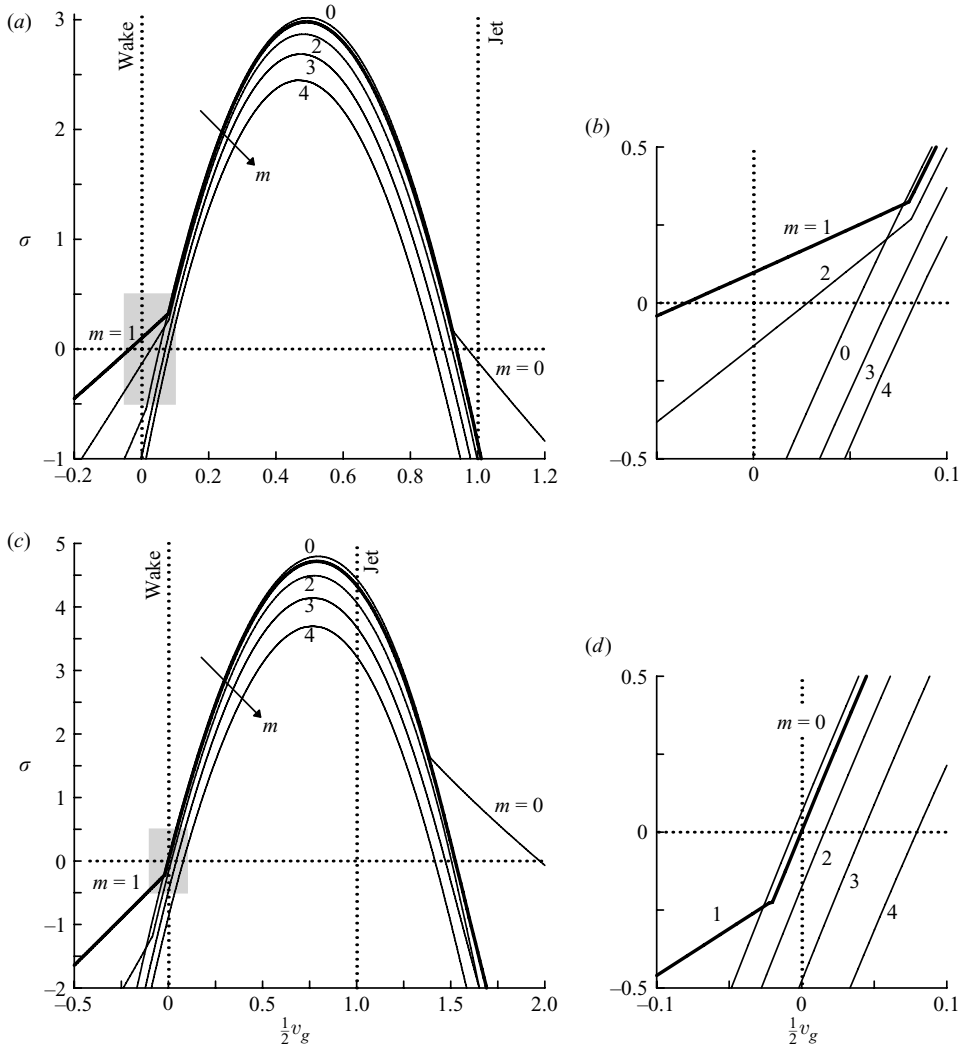

FIGURE 2. Spatio-temporal growth rates σ of the helical mode $m=1$ (thick line), and of the modes of azimuthal wavenumbers $m=0, 2, 3, 4$ (thin lines), for $D/\theta=60$, $M_\infty=0$ and $Re_\infty=2000$. When the trailing edge of a wave packet ($\sigma=0$) extends over the $v_g=0$ dotted line, the corresponding wake is absolutely unstable. Symmetrically, when the leading edge of the wave packet extends beyond the dotted line $v_g/2=1$, the jet profile associated to $\Lambda^{jet}=-\Lambda^{wake}$ is absolutely unstable. (*a*) Homogeneous wake ($S=1$) for $\Lambda=-1.2$. (*b*) Enlargement of the $v_g=0$ shaded area of (*a*). (*c*) Light wake ($S=0.3$) for $\Lambda=-2.25$. (*d*) Enlargement of the $v_g=0$ shaded area of (*c*).

$m=1$ wave packet is also plotted in figure 3(*b*), all other parameters being identical to that used in figure 3(*a*). For these parameter settings, the angular point corresponds always to a group velocity $v_g>0$. The wake mode wavelength is almost independent of D/θ, so that λ^v rescaled by D/θ varies proportionally to D/θ in figure 3(*b*). The shear-layer mode rescaled wavelength is almost independent of D/θ, confirming that λ^v scales on the momentum thickness θ and is insensitive to curvature effects, a result supporting the idea that this mode is analogous to the disturbances in plane mixing layers, as D/θ goes to infinity.

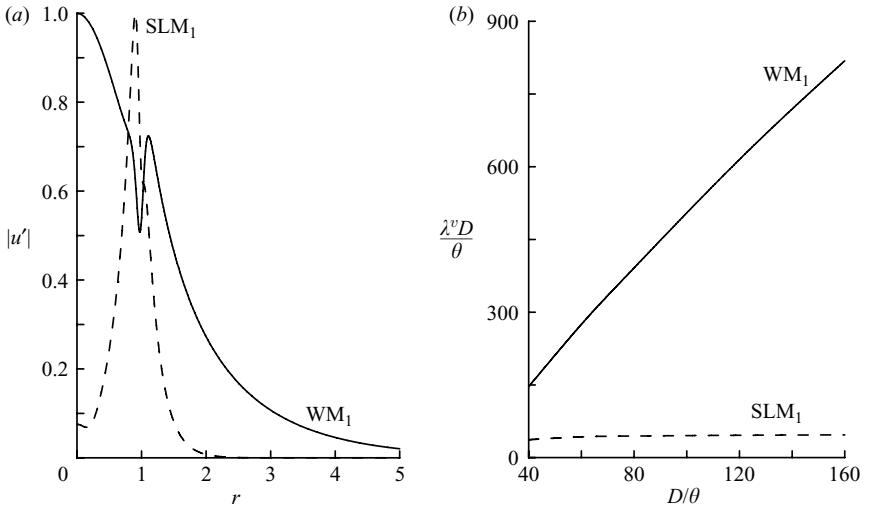

FIGURE 3. $\Lambda = -1.2$, $S = 1$, $M_\infty = 0$ and $Re_\infty = 2000$ and azimuthal wavenumber $m = 1$. (*a*) Normalized radial velocity eigenfunctions for $D/\theta = 60$. Wake mode at $v_g = 0$ (——, WM_1) and shear layer mode at $v_g = 0.15$ (— — —, SLM_1). (*b*) Wavelength λ^v renormalized by the momentum thickness θ as a function of D/θ at the group velocity corresponding to the angular point close to the trailing edge of the $m = 1$ wave packet.

Complete maps $k(\omega)$ obtained for contours parallel to the real axis of the ω-plane (i.e. for different fixed values of ω_i), are presented in figures 4(*a*) and 4(*b*) for $v_g = 0$ and in figure 4(*c*) for $v_g = 0.15$. The saddle points corresponding to the pinching events producing the different instability modes documented in figure 3(*a*) are represented. k_1^- denotes the spatial branch which, by pinching with the k^+ branch, gives rise to a wake mode, and k_2^- its counterpart for the shear-layer mode. The saddle point associated with the k_3^- branch (open diamond symbol) is not considered here, as extensive computations, carried out for different control parameters, show that this point displays the highest absolute growth rate only in cases where it is a non-physical k_2^-/k_3^- point. For $v_g = 0$, the k^+/k^- pinching point of highest absolute growth rate is the wake mode, owing to the pinching of the k^+ and k_1^- branches at $k^0 = 0.625 - 1.401\,\mathrm{i}$, for $\omega^0 = 1.484 + 0.097\,\mathrm{i}$. Note that the k_1^- branch issues from the $k_r < 0$ domain, more clearly visible on the close-up in figure 4(*b*). Studies by Healey (2005, 2006) have warned against the specific dynamics that may be associated with such pinching with branches issuing from the $k_r < 0$ half-domain, i.e. the other side of the branch cut, the other side of the looking glass (Carroll 1872), where eigenmodes grow in the cross-stream direction. Fortunately, in the present case, we observe that the wake mode saddle point remains at a distance $k_r \sim 0.5$ from the $k_r = 0$ axis, which is consistent with the idea that k_r scales on the wake diameter. Therefore, standard results remain valid. If ω_i is decreased further below $\omega_i^0 = 0.097$, the shear-layer mode arises owing to the coalescence of the merged k^+/k_1^- branch with the k_2^- branch. Similar maps $\tilde{k}(\tilde{\omega})$ are presented in figure 4(*c*) for $v_g = 0.15$. In this case, the pinching point of highest absolute growth rate is the shear-layer mode, formed by the pinching of the k^+ and the k_2^- branch at $\tilde{k}^0 = 5.269 - 4.896\,\mathrm{i}$, for $\tilde{\omega}^0 = 5.016 + 2.262\,\mathrm{i}$. If $\tilde{\omega}_i$ is decreased further, the wake mode arises owing to the coalescence of the merged k^+/k_2^- branch with the k_1^- branch. This existence of two distinct helical instability modes resulting from the pinching of a single unstable k^+ branch with two distinct k^- branches is

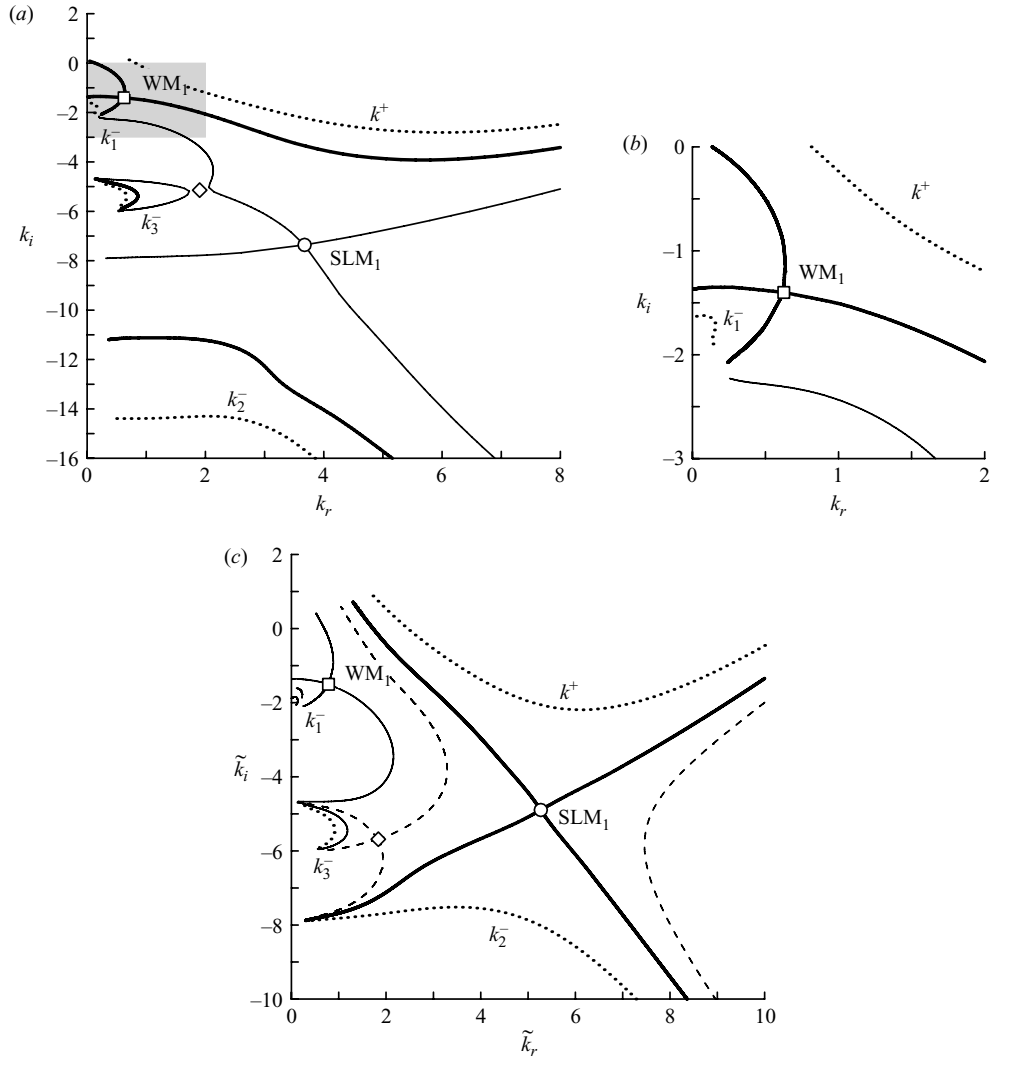

FIGURE 4. Spatio-temporal branches $k(\omega)$ in the complex k-plane for various values of ω_i. $\Lambda = -1.2$, $D/\theta = 60$, $S = 1$, $M_\infty = 0$ and $Re_\infty = 2000$. The WM_1 and SLM_1 labels mark the saddle points associated, respectively, to the wake mode and the shear-layer mode. (*a*) $v_g = 0$. (*b*) Enlargement of the shaded pinching area of (*a*). (*c*) $v_g = 0.15$.

somehow reminiscent of that resulting in the competition between axisymmetric jet column and shear-layer modes in heated jets, documented by Jendoubi & Strykowski (1994), although there is no connection between the leading edge modes of the $m = 0$ wave packet and the trailing edge modes of the $m = 1$ wave packet. Similar results are also discussed in the study of Juniper (2006) on confined two-dimensional jets (see figure 3 for instance).

3.2. *Overall wave packet: azimuthal wavenumber selection*

The spatio-temporal growth rate for axisymmetric disturbances ($m = 0$) is also plotted in figures 2(*a*) and 2(*b*). The angular point close to the leading edge corresponds to the existence of the jet-column modes alluded to above, that lead the convective–absolute

transition for isothermal or hot jets, as discussed in Jendoubi & Strykowski (1994) and Lesshafft & Huerre (2007). At the trailing edge, the $m=0$ spatio-temporal growth rate exhibits a second angular point (barely noticeable in figure 2*b*) corresponding to the existence of axisymmetric wake modes at low group velocities.

The structure of the $m=2$ wave packet is similar to that of the $m=1$ modes, with the possibility of the trailing edge being dominated by a large-scale wake mode (see the close-up of figure 2*a*), but its growth rate is smaller at all group velocities than its $m=1$ counterpart.

For higher azimuthal modes $m>2$, the growth rate for each group velocity decreases as m increases. If the curvature effect is neglected at leading order for this large steepness parameter ($D/\theta=60$), the stabilization of the shear-layer mode for increasing azimuthal wavenumbers may be interpreted as an effect of the Squire theorem, since the misalignment of the local wave vector $m/r\boldsymbol{e}_\theta + k_r\boldsymbol{e}_z$ with the direction of the axisymmetric wave vector $\boldsymbol{e}_z$ increases with m. For the parameter settings of figure 2(*a*), the overall azimuthal wavenumber trailing edge is dominated by the absolutely unstable helical wake mode ($m=1$), whereas the overall leading edge is dominated by the axisymmetric jet column mode ($m=0$). To our knowledge, these results on three-dimensional jets and wakes have never been shown since emphasis was put on jets, and even publications that have shown the entire jet wave packet for both $m=0$ and $m=1$ (Lesshaft & Huerre 2007) have overlooked the possibility of a different mode at the 'wake side' of the wave packet, corresponding to the existence of the wake modes described above. Extensive calculations in the wide range of parameters investigated here suggest that the overall trailing edge can be dominated by the axisymmetric shear-layer mode for sufficiently light wakes. Figure 2(*c*) presents the modification of the wave packet when the density is decreased down to $S=0.3$. The trailing edge of the $m=1$ wave packet is now led by the shear-layer mode, and the overall wave packet is dominated by the $m=0$ shear-layer mode (see the close-up in figure 2*d*). Comparing figures 2(*a*) and 2(*c*), we see at the trailing edge that the angular point of the $m=1$ wave packet has moved to negative growth rates, meaning that lightening the wake stabilizes the helical wake mode. The strong negative value of the velocity ratio Λ used in figure 2(*c*) in order to show the wave packet at the threshold of absolute instability demonstrates that, as in the two-dimensional case (Yu & Monkewitz 1990), the lighter the wake, the stronger the backflow required for the instability to be absolute. The effect is opposite at the leading edge, where the angular point of the $m=0$ wave packet has moved to large growth rates. This is in agreement with the promotion of absolute instability in axisymmetric low-density jets (Jendoubi & Strykowski 1994).

3.3. *Evolution of the largest spatio-temporal growth rate*

The top of the wave packet in figure 2, i.e. the mode of maximum spatio-temporal growth rate σ_{max} is of particular interest since it is identical to the mode of maximum temporal growth rate $\omega_{i,max}$ (Huerre & Rossi 1998). It defines the largest growth rate that may be observed while moving with the perturbation at the velocity v_{gmax} for which $\sigma(v_g)=\sigma_{max}$. Values of σ_{max} have been computed for different values of the steepness parameter D/θ. The results are presented in figure 5, where the smallest physical value of D/θ is 6.5, corresponding to the standard Gaussian velocity profile considered by Batchelor & Gill (1962), which is here recovered for $D/\theta=6.5$ ($N=1$). σ_{max} is asymptotically proportional to D/θ, confirming that the shear-layer mode is closely related to the Kelvin–Helmholtz instability. Consistently with the results previously discussed from figure 2, the $m=0$ and the $m=1$ maximum spatio-temporal

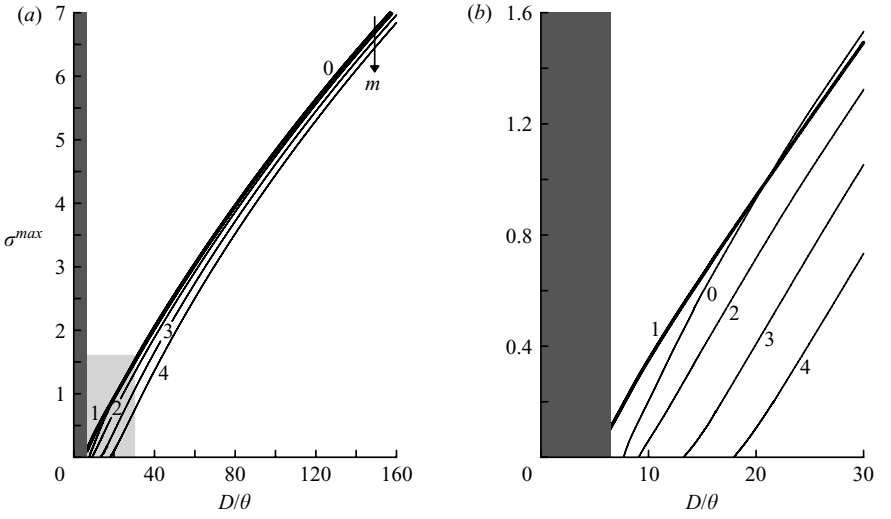

FIGURE 5. (*a*) Maximum spatio-temporal growth rate σ_{max} as a function of D/θ, for the helical mode $m=1$ (thick solid line), and the modes of azimuthal wavenumbers $m=0, 2, 3, 4$. $\Lambda=-1.2$, $S=1$, $M_\infty=0$ and $Re_\infty=2000$. The dark shaded area corresponds to $D/\theta<6.5$, these values not being allowed for profiles defined by (2.6)–(2.7). (*b*) Enlargement of the light shaded area of (*a*).

growth rates are remarkably similar, although the axisymmetric mode is slightly more unstable for $D/\theta \gtrsim 23$. The maximum spatio-temporal growth rate then slowly decreases as m is increased, in agreement with the prediction of the Squire theorem that applies for large steepness parameters. Figure 5(*b*) shows that helical disturbances ($m=1$) are the most amplified for sufficiently small values of D/θ, namely $D/\theta \lesssim 23$, and that only helical disturbances are amplified for $D/\theta \leqslant 8$. Identical results can be found in the analysis of axisymmetric jets by Batchelor & Gill (1962), showing that only helical disturbances are amplified when the shear region of the jet is sufficiently thick. Figure 6 presents the variation of σ_{max} as a function of S and M_∞, for $D/\theta=60$. All azimuthal wavenumbers display a maximum amplification for $M_\infty=0$ and $S\sim 1$. These results are typical of shear instability and have already been documented in the context of plane vortex sheets, see for instance Miles (1958) for the effect of the Mach number and Drazin & Reid (1981) for the effect of the density ratio. Note that the effect of the density ratio on the most amplified spatio-temporal mode contrasts with that described for the edges of the wave packet. Decreasing the density ratio below $S=1$ reduces the maximum spatio-temporal growth rate but accelerates the wave packet, promoting convective instability at the trailing edge ('wake side') and absolute instability at the leading edge ('jet side'). Increasing the density ratio above $S=1$ also reduces the maximum spatio-temporal growth rate, but it slows down the wave packet, promoting absolute instability at the trailing edge and convective instability at the leading edge.

4. Convective–absolute transition

A wake is absolutely unstable if the trailing edge of the linear impulse response propagates at a negative group velocity. Therefore, it is deduced from the previous discussion that the convective–absolute transition is led either by the axisymmetric shear-layer mode $m=0$ (SLM_0) or the helical wake mode $m=1$ (WM_1). In this section,

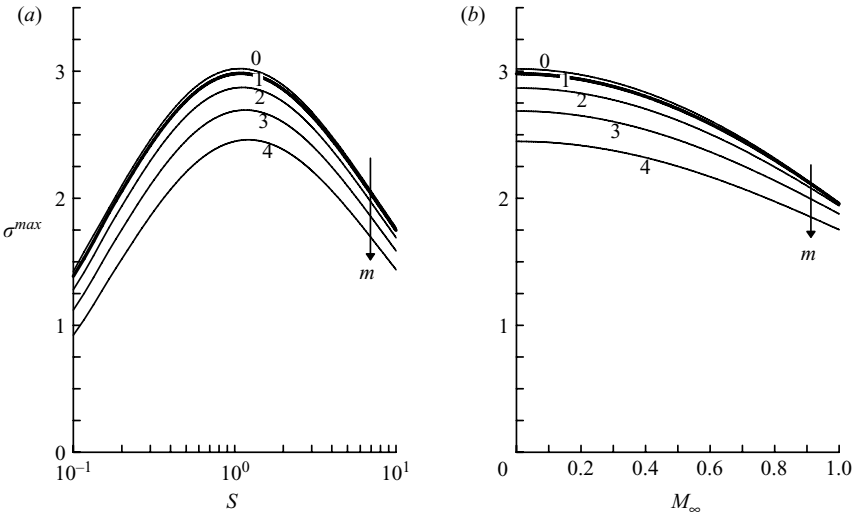

FIGURE 6. Maximum spatio-temporal growth rate σ_{max} of the helical mode $m=1$ (thick solid line), and of the modes of azimuthal wavenumbers $m=0, 2, 3, 4$. $\Lambda=-1.2$, $S=1$, $M_\infty=0$ and $Re_\infty=2000$, (*a*) as a function of the density ratio, at $M_\infty=0$. (*b*) as a function of the Mach number, at $S=1$.

we investigate the convective/absolute transition of axisymmetric wakes, and identify the selected dominant mode that leads the transition in the laboratory frame ($v_g=0$), in a parameter space including the velocity ratio Λ, the steepness parameter D/θ, the density ratio S, and the Mach number M_∞. For simplicity, a control parameter is said to be destabilizing (resp. stabilizing) when its variation results in an extension (resp. reduction) of the domain of absolute instability.

4.1. *Effect of the density ratio*

We study the effect of the density ratio and the velocity ratio on the stability properties of the base flow, for a wake of steepness parameter $D/\theta=60$ at zero Mach number. The boundary of the domain of absolute instability in the (S, Λ)-plane is presented in figure 7. We use a dashed curve when the transition is led by the axisymmetric shear-layer mode and a plain curve when it is led by the helical wake mode. The instability is absolute for combinations of parameters located in the shaded region, labelled AU, and convective for all other combinations of parameters (CU-labelled region).

The absolute instability boundary is reminiscent of that documented by Yu & Monkewitz (1990) in the case of two-dimensional wakes, namely large high (resp. low) density ratios are destabilizing (resp. stabilizing) and promote absolute (resp. convective) instability. A discontinuity in the boundary occurs at $S=0.396$, a point marked by an open circle in figure 7, where the dominant mode switches from the axisymmetric shear-layer mode ($S\leqslant 0.396$) to the helical wake mode ($S\geqslant 0.396$). In the following, this particular point where both modes are simultaneously marginally absolutely unstable is referred to as the crossover point. Note also that the marginal curve crosses the $\Lambda=-1$ line at $S=1.551$. Therefore, wakes with sufficiently high density ratios can be absolutely unstable to $m=1$ perturbations (wake mode), even with a coflow on the axis. The threshold is found to be asymptotic to $\Lambda=-0.9$ as S increases, indicating that the critical velocity ratio depends weakly on the density

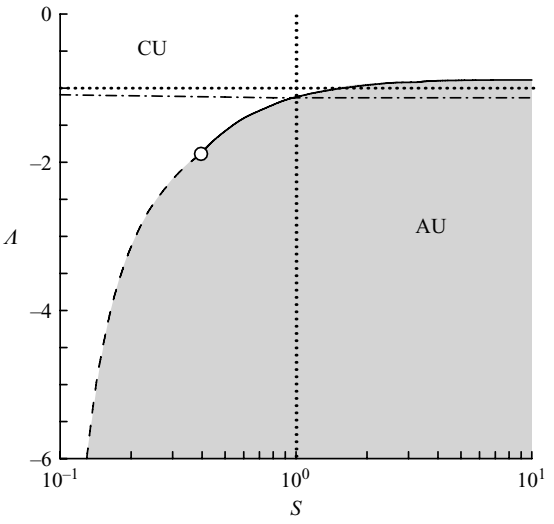

FIGURE 7. Boundary separating the regions of absolute (shaded domain labelled AU) and convective (domain labelled CU) instability in the (S, Λ)-plane, for $D/\theta = 60$, $M_\infty = 0$ and $Re_\infty = 2000$. The transition to absolute instability is led either by the axisymmetric shear-layer mode (dashed line) or the helical wake mode (solid line). The open circle marks the crossover point corresponding to the change in the selection of the dominant mode. The dash-dotted line is the curve of marginal absolute instability in the absence of baroclinic effects.

ratio: for instance, absolute instability occurs in presence of a coflow rate of 5.3% at $S = 10$ and of 5.8% at $S = 4$. On the contrary, for low density ratios, the critical velocity ratio required to reach absolute instability is dramatically affected by small variations of S: for instance, absolute instability occurs in presence of a counterflow rate of 22.5% at $S = 0.5$ and of 51.7% at $S = 0.2$.

This striking behaviour may be understood by considering the effect of the baroclinic torque, as first suggested by Soteriou & Ghoniem (1995) for the stability of homogeneous and non-homogeneous shear layers. The main idea is that a baroclinic torque arising from base flow density gradients and from the pressure perturbations $\boldsymbol{\Gamma} = (\nabla\rho_0 \times \nabla p')/\rho_0^2$ can act as a source for the vorticity perturbations, as discussed by Nichols *et al.* (2007) in the case of non-homogeneous round jets, for instance. On similar jet configurations, Lesshafft & Huerre (2007) have shown that the impact of baroclinic effects can be assessed by solving a modified dispersion relation, in which the linearized momentum equations are artificially forced in order to cancel the baroclinic torque, which has only one non-trivial component $\Gamma_\theta \boldsymbol{e}_\theta$ due to the axisymmetry. This method is generalized here to the case of non-axisymmetric disturbances, leading to a two-component baroclinic torque $\Gamma_\theta \boldsymbol{e}_\theta + \Gamma_z \boldsymbol{e}_z$, where

$$\Gamma_\theta = \mathrm{i}k^0 \frac{\partial_r \rho_0}{\rho_0^2} p'(r) \mathrm{e}^{(\mathrm{i}k^0 z + m\theta - \omega^0 t)}, \tag{4.1a}$$

$$\Gamma_z = -\mathrm{i}\frac{m}{r} \frac{\partial_r \rho_0}{\rho_0^2} p'(r) \mathrm{e}^{(\mathrm{i}k^0 z + m\theta - \omega^0 t)}, \tag{4.1b}$$

Γ_z being non-zero for $m \neq 0$. More details on the vorticity equations can be found in Appendix B. The absolute instability boundary associated to the modified dispersion relation, where the two-component baroclinic torque has been cancelled, is shown in figure 7 (dash-dotted line). When the baroclinic effects are removed, the transition from

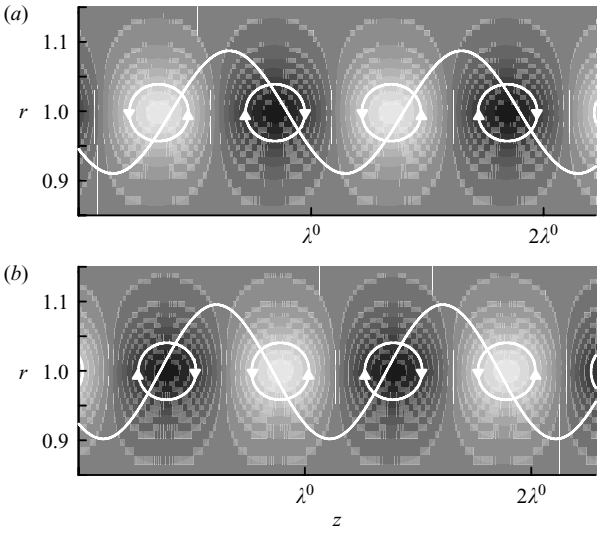

FIGURE 8. (*a*) Displacement $\eta(r=1,\theta=0,z)$ (drawn with an arbitrary finite amplitude) and baroclinic torque Γ_t associated to the marginally absolutely unstable eigenmode, projected along the vector $\boldsymbol{t}(r=1)$ tangent to the phase lines of η, for $S=2.5$. The rotation induced by the torque is visualized by the white circles with arrows. ($D/\theta=60$, $M_\infty=0$ and $Re_\infty=2000$). (*b*) Same as (*a*) but for $S=0.45$. This figure extends to non-axisymmetric perturbations the arguments of Lesshafft & Huerre (2007) and Nichols *et al.* (2007) (see their figures 5 and 8, respectively).

convective to absolute instability is led by the helical wake mode ($m=1$) whatever the value of the density ratio. For $S=1$, forced and unforced marginal absolute instability curves cross since the baroclinic torque vanishes in the homogeneous case. Surprisingly, the convective–absolute transition is nearly independent of S when the baroclinic torque is cancelled, even though the density ratio still enters the dispersion relation, the relative difference not being measurable for $S>1$, and being negligible for $S<1$ (0.9% at $S=0.5$ and 3.5 % at $S=0.1$). It may therefore be concluded that the baroclinic torque $\boldsymbol{\Gamma}$ promotes the onset of absolute instability in heavy wakes and delays it in light wakes. The physical mechanism proposed by Lesshafft & Huerre (2007) to explain the stability of axisymmetric disturbances in hot jets may be extended to non-axisymmetric perturbations by examining how the baroclinic torque associated with the spatio-temporal absolute eigenmode interacts with the associated displacement η of the shear layer at $r=1$, computed from the radial velocity perturbation as $\partial_t\eta + W\partial_z\eta = u'$, so that

$$\eta = \frac{-\mathrm{i}u'}{k^0 W_b - \omega^0}. \tag{4.2}$$

Considering the vector tangent to the phase lines of η, defined as $\boldsymbol{t}=k_r^0\boldsymbol{e}_\theta - m/r\boldsymbol{e}_z$, only the component of the baroclinic torque along $\boldsymbol{t}$

$$\Gamma_t = \boldsymbol{\Gamma}\cdot\frac{\boldsymbol{t}}{\|\boldsymbol{t}\|} \tag{4.3}$$

plays a role in the displacement of the shear layer. Figure 8(*a*) shows the shear-layer displacement and the spatial distribution of Γ_t in a meridional plane, computed for the helical wake mode at the absolute instability threshold, for a heavy wake of ratio $S=2.5$. All spatial amplifications are neglected for clarity by setting the spatial

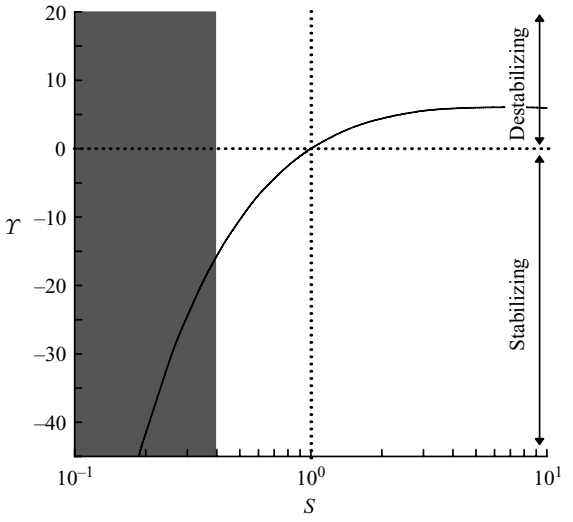

FIGURE 9. Baroclinic factor Υ at the absolute instability threshold, i.e. along the curve $\Lambda(S)$ plotted in figure 7, valid only in the non-shaded area where the wake mode leads the absolute transition ($D/\theta = 60$, $M_\infty = 0$ and $Re_\infty = 2000$). In the shaded area are reported the values of Υ of the mode associated with the wake mode saddle point, followed by continuity.

growth rate $-k_i^0$ to zero. Results are reminiscent of that documented in Lesshafft & Huerre (2007) and Nichols *et al.* (2007): the baroclinic torque is concentrated within the shear layer, in regions of alternating sign. The baroclinic torque is destabilizing since it induces a clockwise rotation when η decreases with z, and a counterclockwise rotation when η increases with z. This effect of the baroclinic torque is thus determined by the relative phase ϕ of the projected torque Γ_t, evaluated in the shear layer ($r = 1$), with respect to the displacement η

$$\phi = \arg\{\Gamma_t|_{r=1}\} - \arg\{\eta|_{r=1}\}. \tag{4.4}$$

Because there is almost a quadrature advance between Γ_t and η ($\phi = 1.90$), the baroclinic torque tends to enhance the deformation of the shear layer, and is therefore destabilizing, as indeed is predicted by the direct stability analysis. Figure 8(*b*) shows similar results for a light wake of density ratio $S = 0.45$, but owing to the change of sign of the base flow density gradient, we find in that case a quadrature delay between Γ_t and η ($\phi = -1.77$), so that Γ_t now induces stabilizing deformations that oppose the shear-layer deformation. These results, generalizing the argument of Lesshafft & Huerre (2007) to the case of non-axisymmetric disturbances, show that the action of the baroclinic torque may result in an increase or in a decrease of the instability growth rate. This baroclinic effect depends on the magnitudes of Γ_t and on its relative phase ϕ with the displacement η: the stabilizing (resp. destabilizing) effect is maximum when ϕ is $-\pi/2$ (resp. $\phi = \pi/2$). When ϕ is close to 0 or π, the leading-order effect of the torque is neutral, as it then displaces upstream or downstream the shear-layer undulation. Therefore, we propose to cast the effect of the baroclinic torque in the single baroclinic factor

$$\Upsilon = \sin\phi \left|\frac{\Gamma_t}{\eta}\right|_{r=1}, \tag{4.5}$$

i.e. we consider baroclinic effects for a fixed amplitude of the displacement. Figure 9 shows the calculated value of Υ at the absolute instability threshold of the helical

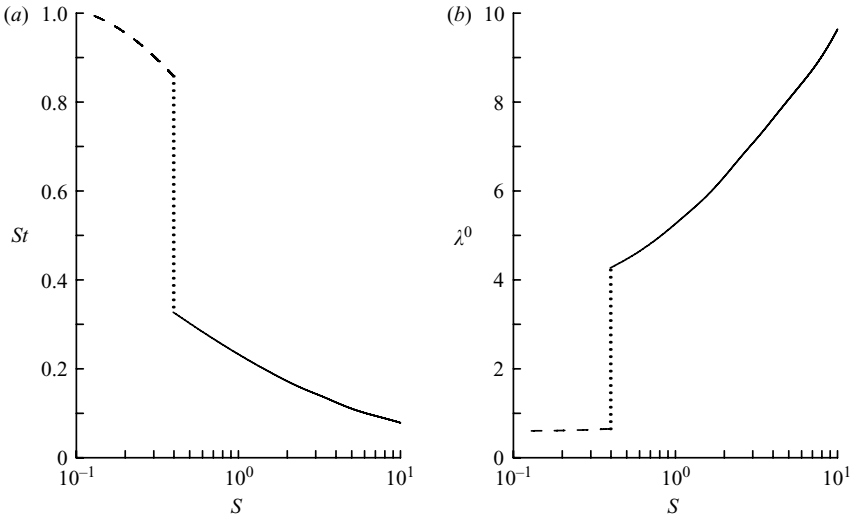

FIGURE 10. (*a*) Strouhal number St and (*b*) absolute wavelength λ^0 as a function of the density ratio at the absolute instability threshold. $D/\theta = 60$, $M_\infty = 0$ and $Re_\infty = 2000$. The curve is dashed when the transition is led by the axisymmetric shear-layer mode, and solid when it is led by the helical wake mode.

wake mode. In agreement with the results discussed from figure 7, values of Υ indicate a destabilizing effect of the baroclinic torque for $S > 1$ (positive values), and a strong baroclinic stabilization as S decreases to zero (low negative values).

Figure 10 presents the Strouhal number St and wavelength λ^0 as a function of the density ratio at the absolute instability threshold, i.e. for parameter couples (S, Λ) varying along the boundary of the absolutely unstable domain shaded in figure 7. At the crossover ratio $S = 0.396$, both curves undergo a brutal discontinuity, owing to the change in the selection of the dominant mode, from the axisymmetric shear-layer mode to the helical wake mode. When the density ratio increases in the range $0.1 \leqslant S \leqslant 0.396$, the axisymmetric shear-layer mode dominates: the absolute wavelength remains constant, of order 0.5 wake diameter, and the absolute frequency is high and decreases from 1 to 0.9. When S is increased above 0.396, the helical wake mode dominates: the absolute wavelength jumps to 4 wake diameters and grows up to 10 diameters. At the same time, the absolute frequency drops to 0.3 and keeps decreasing to 0.1 at $S = 10$.

4.2. *Effect of the steepness parameter*

We investigate the effect of varying the steepness parameter on the absolute instability threshold of the flow, keeping $M_\infty = 0$.

Figure 11 presents absolute instability boundaries when the steepness parameter varies within the range $40 \leqslant D/\theta \leqslant 160$. The crossover points between the axisymmetric shear-layer mode and the helical wake mode are marked by an open circle. All curves reflect the same trend as for $D/\theta = 60$ (figure 7). The steepness parameter has essentially no effect at high density ratios, where the helical wake mode leads the transition. However, at low density ratios, increasing the steepness parameter has a stabilizing effect, and the domain of absolute instability shrinks significantly. The density ratio at the crossover point monotonically increases with D/θ, from 0.202 at $D/\theta = 40$ to $S = 0.673$ at $D/\theta = 160$, whereas at the same time, the rate of

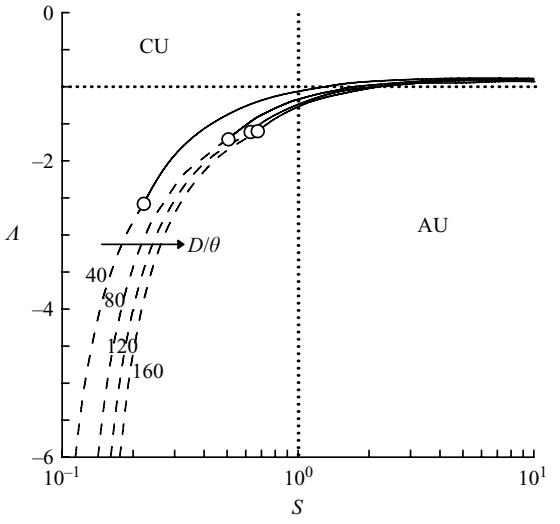

FIGURE 11. Boundary separating the regions of absolute (AU) and convective (CU) instability and crossover points (○) in the (S, Λ)-plane for the steepness parameters 40, 80, 120 and 160, at $M_\infty = 0$ and $Re_\infty = 2000$ (– – –, SLM_0; ———, WM_1).

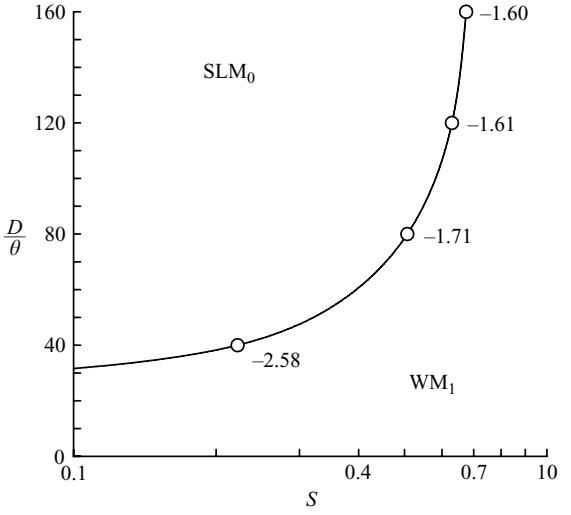

FIGURE 12. Locus of the crossover point in the $(S, D/\theta)$-plane, for $M_\infty = 0$ and $Re_\infty = 2000$. This curve separates domains where the transition to absolute instability is led, respectively, by the axisymmetric shear-layer mode (domain labelled SLM_0) and the helical wake mode (domain labelled WM_1). Open circles correspond to the crossover points for the four values of D/θ plotted in figure 11 and are labelled here with their corresponding velocity ratio Λ.

counterflow necessary to reach absolute instability decreases from 48.6% ($\Lambda = -2.89$) to 23.4% of the free-stream velocity ($\Lambda = -1.61$). This effect is synthesized in figure 12, which shows the variations of the density ratio at the crossover point as a function of D/θ. Values of the critical velocity ratios Λ below which the instability becomes absolute are reported along the crossover curve for the four values of D/θ presented in figure 11. The axisymmetric shear-layer mode is dominant for combinations of parameters located above the curve (region labelled SLM_0), and the helical wake

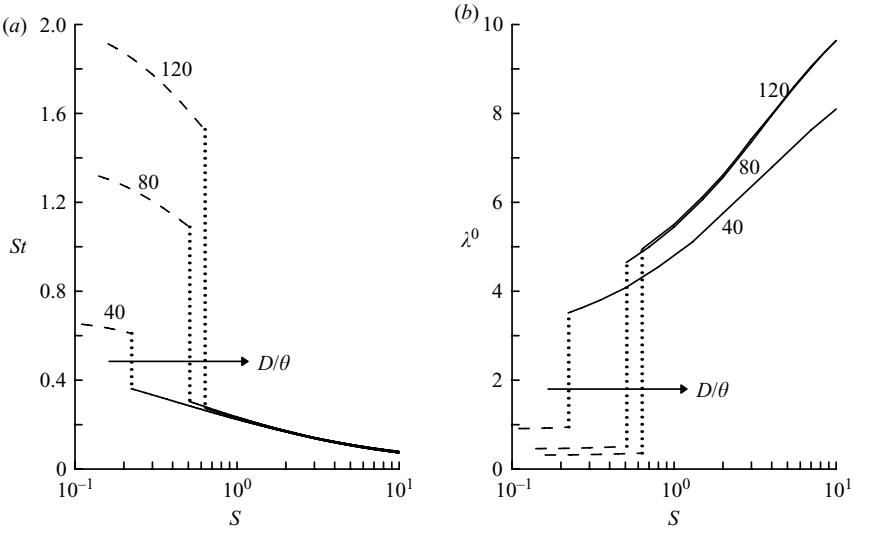

FIGURE 13. (*a*) Strouhal number St and (*b*) absolute wavelength λ^0 at the absolute instability threshold for steepness parameters $D/\theta = 40$, 80 and 120. $M_\infty = 0$ and $Re_\infty = 2000$ (— — —, SLM_0; ———, WM_1).

mode is dominant for parameters located below the curve (region labelled WM_1). The convective–absolute transition is essentially led by the helical wake mode, the axisymmetric shear-layer mode being dominant only at low density ratios and large steepness parameters. For small values of the steepness parameter $D/\theta \leqslant 32$, the helical wake mode is dominant for all density ratios $0.1 \leqslant S \leqslant 10$ considered in this study. Note that in the homogeneous case ($S = 1$), the absolute instability is led by the helical wake mode for all steepness parameters, as reported in Monkewitz (1988) for incompressible homogeneous wakes. Figure 13 shows the Strouhal number and wavelength at the absolute instability threshold for different values of the steepness parameter D/θ. The curve trends are similar to that presented in figure 10, namely the frequency and the wavelength respectively increases and decreases when the density ratio increases, and all curves are discontinuous at the crossover point characterizing the change in the selection of the dominant mode. For low values of S, the axisymmetric shear-layer mode is dominant and selects high frequencies increasing with D/θ ($St \sim 0.6$ for $D/\theta = 40$ and $1.5 \leqslant St \leqslant 1.9$ for $D/\theta = 120$), and short wavelengths decreasing with D/θ (of order 0.9 wake diameter for $D/\theta = 40$ and 0.3 wake diameter for $D/\theta = 120$, these values being almost independent of S). For higher values of S, the helical wake mode is dominant and is characterized by low frequencies $0.1 \leqslant St \leqslant 0.4$ depending on S, but almost independent of the steepness parameter, and by large wavelengths varying between 4 and 10 wake diameters, the values obtained for $D/\theta = 80$ and 120 being equal.

The behaviour is different for smaller values of the steepness parameter. We present in figure 14 the absolute instability threshold in the range $D/\theta \leqslant 15$. For all values of D/θ in that range and for all density ratios, convective–absolute transition is led by the helical wake mode, a result consistent with that discussed from figure 12. In opposition to the behaviour described in figure 11, lowering D/θ has a stabilizing effect for all density ratios S, and it results in a significant reduction of the absolutely unstable region. In particular, absolute instability requires counterflowing streams at

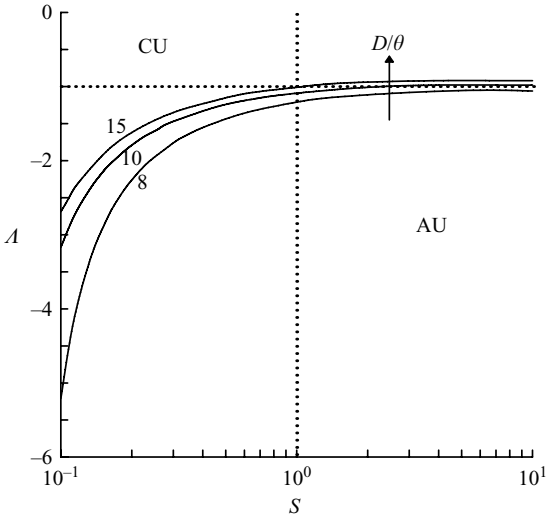

FIGURE 14. Boundary separating the regions of absolute (AU) and convective (CU) instability in the (S, Λ)-plane for $D/\theta = 8$, 10 and 15, at $M_\infty = 0$ and $Re_\infty = 2000$. For these values of the steepness parameter, the transition is led by the helical wake mode only (no crossover point in the domain).

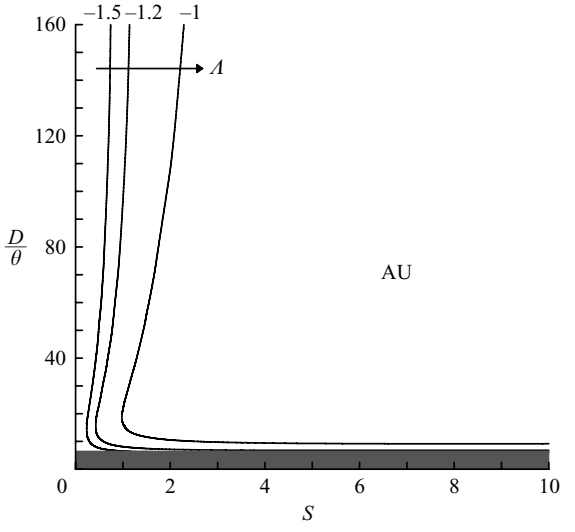

FIGURE 15. Absolutely unstable domains (AU) in the $(S, D/\theta)$-plane for three velocity ratios $\Lambda = -1$, -1.2 and -1.5, at $M_\infty = 0$ and $Re_\infty = 2000$. For these values of Λ, the transition is led by the helical wake mode only (no crossover point in the domain). The shaded area corresponds to $D/\theta < 6.5$, these values not being allowed for profiles defined by (2.6)–(2.7).

$D/\theta = 8$, even for heavy wakes, since the critical velocity ratios are located in this case below $\Lambda = -1$ for all values of S.

The stability properties of the helical wake mode are further investigated by considering regions of absolute and convective instability in the $(S, D/\theta)$-plane for different values of Λ. Figure 15 presents the absolute instability boundaries obtained for $\Lambda = -1.5, -1.2$, and -1, corresponding to counterflow rates of 20%, 9.1% and zero. Note that since velocity ratios below -1.61 are required for the axisymmetric

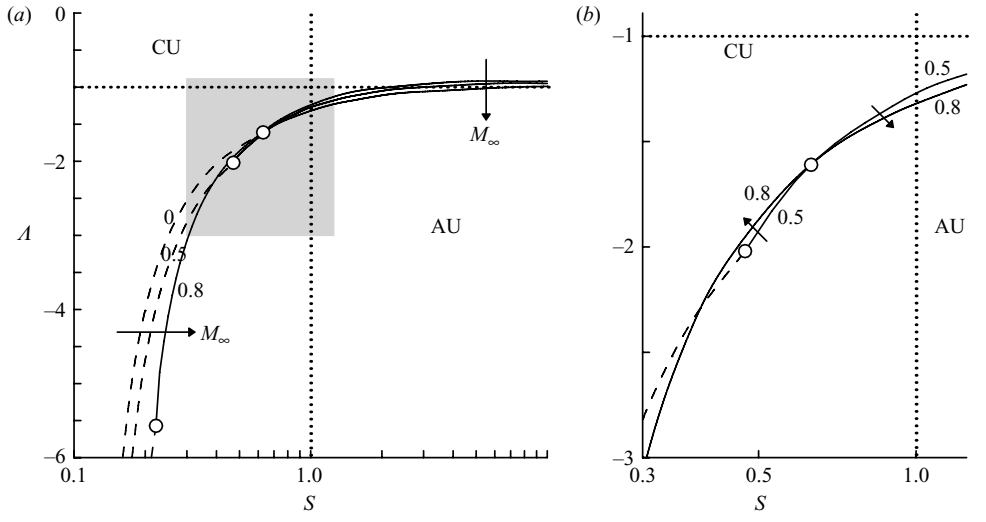

FIGURE 16. (*a*) Boundary separating the regions of absolute (AU) and convective (CU) instability and crossover points (○) in the (S, Λ)-plane for the Mach numbers $M_\infty = 0$, 0.5 and 0.8, at $D/\theta = 120$ and $Re_\infty = 2000$ (– – –, SLM_0; ———, WM_1). (*b*) Enlargement of the shaded area of (*a*). The $M_\infty = 0$ curve has been removed for clarity.

shear-layer mode to be dominant (see figure 12), the transition to absolute instability is led by the helical wake mode for all the values of Λ presented in figure 15. In the absence of counterflow ($\Lambda \geqslant -1$), the lowest density ratio at which an absoluteinstability exists is $S = 0.982$, for $D/\theta = 19$. For each value of Λ, the critical density ratio for the helical wake mode increases slightly when D/θ varies from 30 to 160, a behaviour corresponding to the stabilizing effect discussed from figure 11. The trend is reversed when D/θ is decreased further below 15, as the critical density ratio increases significantly, illustrating the stabilizing effect shown in figure 14. For $\Lambda = -1$ (resp. $\Lambda = -1.2$), wakes with steepness parameters $D/\theta \lesssim 9$ (resp. $D/\theta \lesssim 7$) are found to be convectively unstable for all density ratios (part of the curves parallel to the S-axis in figure 15). For $\Lambda = -1.5$, absolute instability can be reached by increasing sufficiently the density ratio, even for the smallest steepness parameter $D/\theta = 6.5$ accessible through profiles (2.6). This means that for $\Lambda = -1.5$, the Gaussian wake (associated to $D/\theta = 6.5$ and $N = 1$) is absolutely unstable for $S \geqslant 1.14$, whereas for $\Lambda = -1.2$ or larger, it is convectively unstable for all values of the density ratios.

4.3. *Effect of the free stream Mach number*

We consider now the effect of the Mach number on the stability properties of the flow. Our calculations show that the effect of compressibility is negligible for free-stream Mach numbers below 0.3, the variations of the critical parameters being less than 10%. Figure 16(*a*) presents the absolute instability boundaries in the (S, Λ)-plane for $D/\theta = 120$ and $M_\infty = 0, 0.5$ and 0.8. In the homogeneous case ($S = 1$), increasing the Mach number to high subsonic values is seen to weakly stabilize the helical wake mode, in agreement with the intuitive idea that compressibility slows down the upstream propagation of disturbances and therefore favours convective instability. A similar stabilizing effect is observed on the helical make mode when $S \gtrsim 0.65$, and for light wakes when the axisymmetric shear-layer mode is dominant. This stabilizing effect of compressibility on the shear-layer mode is consistent with the analysis of

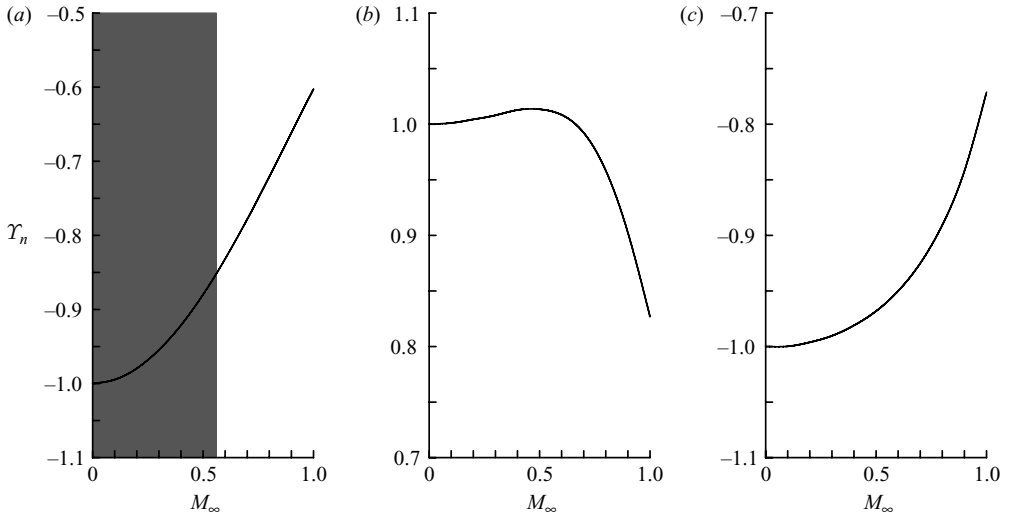

FIGURE 17. Effect of the Mach number on the normalized baroclinic factor Υ_n at the absolute instability threshold, for $D/\theta = 120$ and $Re_\infty = 2000$. (*a*) Helical wake mode for $S = 0.5$, valid only in the non-shaded area where the wake mode leads the absolute transition for this density ratio. In the shaded area are reported the values of Υ_n of the mode associated with the wake mode saddle point, followed by continuity. (*b*) Helical wake mode for $S = 2$ (for this value of S, the transition is led by this mode only). (*c*) Axisymmetric shear-layer mode for $S = 0.2$ (for this value of S, the transition is led by this mode only).

Pavithran & Redekopp (1989) on plane mixing layers. For $S \lesssim 0.65$, the helical wake mode is destabilized by an increase of the Mach number (solid lines in figure 16(*b*) when this mode is dominant), a behaviour in contrast with that of the axisymmetric jet column modes, for which convective instability is promoted by increasing the Mach number in the high subsonic regime, for all values of S (Monkewitz & Sohn 1988; Jendoubi & Strykowski 1994). We propose to interpret these different compressibility effects for light and heavy wakes as the result of a competition between the classical stabilizing effect due to the decrease in the pressure wave speed, and baroclinic effects discussed in § 4.1. Results are given in terms of the baroclinic factor Υ defined by (4.5), normalized by the magnitude of the baroclinic factor of the incompressible wake

$$\Upsilon_n(M_\infty, S, \Lambda, D/\theta, Re) = \frac{\Upsilon(M_\infty, S, \Lambda, D/\theta, Re)}{|\Upsilon(M_\infty = 0, S, \Lambda, D/\theta, Re)|}, \tag{4.6}$$

so that $\Upsilon_n(M_\infty = 0) = \pm 1$. Figure 17 shows the evolution of Υ_n as a function of the Mach number for wakes of different density ratios. The case of a moderately light wake of density ratio $S = 0.5$ is presented in figure 17(*a*), where the transition is led by the helical wake mode for $M_\infty \geqslant 0.63$. The increase of the negative baroclinic factor corresponds to a decrease of the stabilizing effect at this density ratio, i.e. to a destabilization. This suggests that the absolute instability triggered by an increase of the Mach number arises from a weakening of the stabilizing baroclinic torque. Figure 17(*b*) shows the case of a heavy wake of ratio $S = 2$, where the transition is led by the helical wake mode for all Mach numbers. The baroclinic torque remains positive and almost constant until $M_\infty \leqslant 0.5$ and then decreases rapidly, inducing a decrease of the destabilizing effect at this density ratio, i.e. a stabilization consistent with the effect observed in figure 16. The case of a very light wake of density ratio

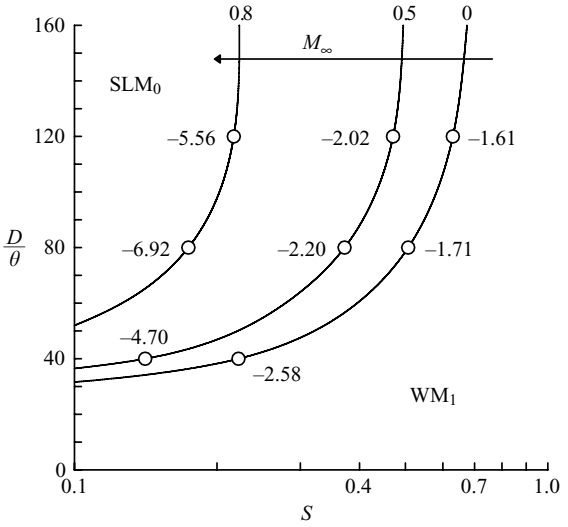

FIGURE 18. Crossover curves in the $(S, D/\theta)$-plane for three values of the Mach number, at $Re_\infty = 2000$. Curves separate domains where the transition to absolute instability is led, respectively, by the axisymmetric shear-layer mode (SLM_0) and the helical wake mode (WM_1). Open circles at $D/\theta = 120$ correspond to the crossover points of figure 16 and are plotted together with their corresponding velocity ratio Λ.

$S = 0.2$ is presented in figure 17(*c*), the transition being led by the axisymmetric shear-layer mode for all Mach numbers. The results are similar to those obtained for the $S = 0.5$ wake, namely the baroclinic effect is destabilizing. Therefore, the global stabilizing effect observed in figure 16 for the shear-layer mode does not result from a variation of the baroclinic torque and should be blamed on the decrease in the disturbance wave speeds when the Mach number is increased.

As a result of the stabilizing effect of the Mach number on the axisymmetric shear-layer mode, and of its destabilizing effect on the helical wake mode for light wakes, the crossover point is displaced in the region of very low density ratios as M_∞ is increased (figure 16). The corresponding critical velocity ratio drops to very small values, illustrating the necessity of strong counterflows to achieve the transition to absolute instability at large M_∞ and small S. For instance, at $M_\infty = 0$, the crossover density ratio is $S = 0.625$ with a critical counterflow rate of 23.7% of the free-stream velocity ($\Lambda = -1.62$). At $M_\infty = 0.8$, the crossover density ratio is $S = 0.215$ with a critical counterflow rate of 70.1% ($\Lambda = -5.70$).

This tendency is visible in figure 18, which generalizes the results presented in figure 12 to Mach numbers $M_\infty = 0.5$ and 0.8. Values of the velocity ratio at the crossover point are reported for the same values of D/θ as in figure 12. Consistently with the results presented in figure 16, the helical wake mode ($m = 1$) is promoted as the dominant mode for high subsonic Mach numbers, this effect being more pronounced for large values of D/θ. For small values of D/θ, the helical wake mode leads the transition to absolute instability at all density ratios, a trend already documented for $M_\infty = 0$.

Figure 19 presents the effect of the Mach number on the critical Strouhal number St and wavelength λ^0 at the absolute instability threshold for different values of the Mach number, at $D/\theta = 120$. The frequency of both modes are lowered at high subsonic Mach numbers, whereas the wavelength increases slightly. For the

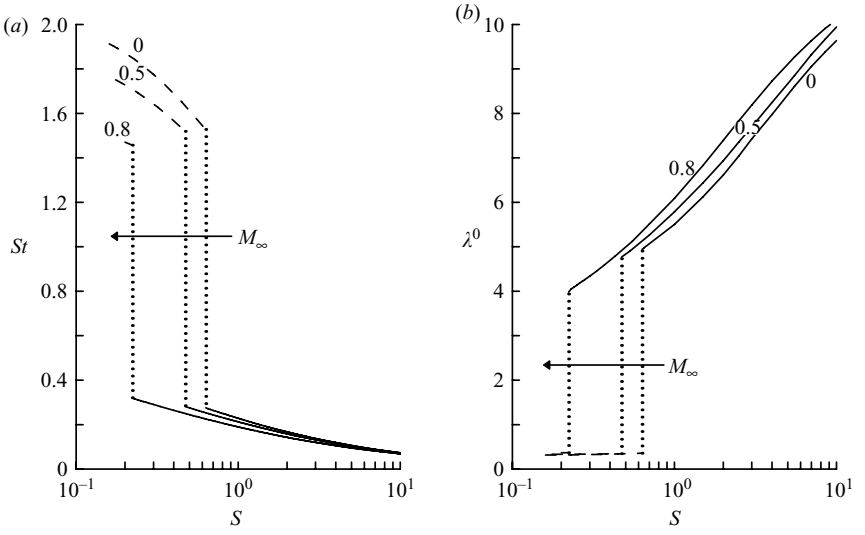

FIGURE 19. (*a*) Strouhal number St and (*b*) absolute wavelength λ^0 at the absolute instability threshold for Mach numbers $M_\infty = 0$, 0.5 and 0.8, i.e. along the curves $\Lambda(S)$ plotted in figure 16. $D/\theta = 120$ and $Re_\infty = 2000$ (– – –, SLM_0; ———, WM_1).

axisymmetric shear-layer mode, we hence find values of approximately $St \sim 1.8$ for $M_\infty = 0$ and ~ 1.5 for $M_\infty = 0.8$, with wavelengths of order 0.3 wake diameter. For the helical wake mode, we find Strouhal numbers $0.1 \leqslant St \leqslant 0.3$, with wavelengths varying between 4 and 10 wake diameters.

The properties of the helical wake mode are finally investigated by considering the combined effect of M_∞ and S in the particular configuration of zero centreline velocity ($\Lambda = -1$). The absolute instability boundaries in the (S, M_∞)-plane are presented in figure 20 for different values of D/θ. Since the axisymmetric shear-layer mode requires a counterflow to become absolutely unstable, the helical wake mode leads the transition for all the combinations of parameters examined here. For all values of the steepness parameter, the range of absolutely unstable density ratios is significantly reduced by increasing the Mach number. For instance, in the range of density ratios under consideration, the lowest steepness parameter at which an absolute instability exists is $D/\theta = 12$ for $M_\infty = 0.9$, and $D/\theta = 9$ for $M_\infty = 0$. Note that the region of absolute instability, quite limited for $D/\theta = 10$, extends dramatically when D/θ is increased to 20, and then shrinks again when D/θ is further increased from 20 to 160. This behaviour is associated to the non-trivial effect of D/θ described for $M_\infty = 0$ in § 4.2, both destabilizing and stabilizing effects being more pronounced as the Mach number increases. For instance, in the range of density ratios under investigation, no absolute instability occurs for Mach numbers above 0.615 at $D/\theta = 10$, and above 0.773 at $D/\theta = 160$.

5. Conclusion

The convective–absolute transition in axisymmetric wakes has been investigated for a fixed Reynolds number $Re_\infty = 2000$, in a parameter space including the velocity and density ratios, the steepness parameter and the free-stream Mach number. Depending on the parameter settings, i.e. to the flow regime, the transition to absolute instability is led either by a large-scale helical wake mode of azimuthal wavenumber $m = 1$, or by a

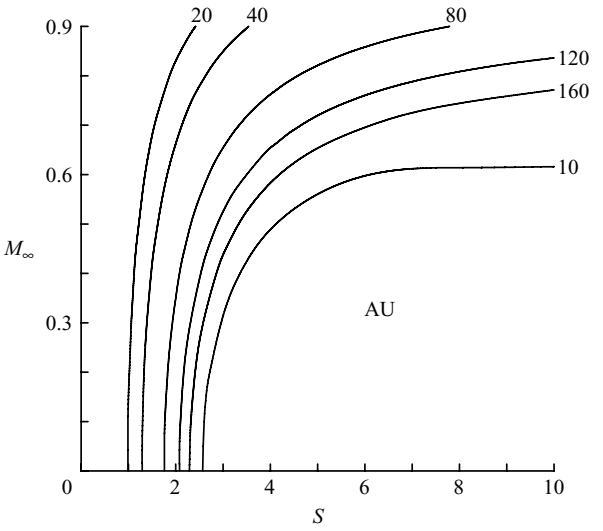

FIGURE 20. Absolutely unstable domains (AU) in the (S, M_∞)-plane as a function of D/θ, at $\Lambda = -1$ and $Re_\infty = 2000$. For this value of Λ, the transition is led by the helical wake mode only (no crossover point in the domain).

small-scale axisymmetric shear-layer mode ($m = 0$). An increase of the density ratio or an increase of the velocity ratio promotes absolute instability, no matter which mode leads the transition. Varying the Mach number has a more complex effect. For very light or heavy wakes, increasing the Mach number promotes convective instability, but for intermediate values of the density ratio, an increase of the Mach number promotes an absolute instability of the helical wake mode, a behaviour strikingly different from that documented for other shear flows. We show that this behaviour may be attributed to the effect of the baroclinic torque. The axisymmetric shear-layer mode is dominant only for low density ratios and high rates of counterflow on the wake axis (large negative velocity ratios). In all other cases, and in particular for small rates of coflow or counterflow more realistic of a real afterbody wake, the transition to absolute instability is led by the helical wake mode. The frequency of the helical wake mode at the absolute instability threshold is weakly dependent on the parameters, and is characterized by Strouhal numbers varying in the range $0.1 \leqslant St \leqslant 0.3$. These results give credence to the interpretation of the large-scale oscillation observed in the experimental studies of flows past spheres, disks and more complex axisymmetric afterbodies in terms of a nonlinear global mode triggered by a local transition to absolute instability. In the whole range of parameters explored here, the azimuthal wavenumber and frequency selection is in qualitative agreement with such a mode made of a front located at the upstream boundary of the absolutely unstable region (separated or not from the body), and followed by a saturated wavetrain (Couairon & Chomaz 1999; Pier 2002). In that case, the front region is the wavemaker and imposes its azimuthal wavenumber and frequency to the entire flow.

The authors acknowledge the financial support of CNES (the French Space Agency) and ONERA (the French Aerospace Lab) within the framework of the research and technology program Aerodynamics of Nozzles and Afterbodies.

Appendix A. Linearized equations of motion

The set of equations is presented for the eigenfunction (ρ', u', v', w', t').

$$(kW_b-\omega)\rho'+\left[d_r\rho_b+\rho_b\left(d_r+\frac{1}{r}\right)\right](-\mathrm{i}u')+m\frac{\rho_b}{r}v'+k\rho_b w'=0, \tag{A 1a}$$

$$-\frac{1}{\gamma M^2}(d_rT_b+T_bd_r)\rho'+(kW_b-\omega)\rho_b(-\mathrm{i}u')-\frac{1}{\gamma M^2}(d_r\rho_b+\rho_bd_r)t'$$
$$=\frac{-\mathrm{i}}{Re}\left[\left(\frac{4}{3}d_{rr}+\frac{4}{3r}d_r-\frac{4+3m^2+3k^2r^2}{3r^2}\right)(-\mathrm{i}u')+\frac{m}{3r}\left(d_r-\frac{7}{r}\right)v'+\frac{k}{3}d_rw'\right], \tag{A 1b}$$

$$\frac{mT_b}{\gamma M^2r}\rho'+\rho(kW_b-\omega)v'+\frac{m\rho_b}{\gamma M^2r}t'$$
$$=\frac{-i}{Re}\left[-\frac{m}{3r}\left(d_r+\frac{7}{r}\right)(-iu')+\left(d_{rr}+\frac{1}{r}d_r-\frac{3+4m^2+3k^2r^2}{3r^2}\right)v'-\frac{mk}{3r}w'\right] \tag{A 1c}$$

$$\frac{kT_b}{\gamma M^2}\rho'+\rho_bd_rW_b(-iu')+\rho(kW_b-\omega)w'+\frac{k\rho_b}{\gamma M^2}t'$$
$$=\frac{-\mathrm{i}}{Re}\left[-\frac{k}{3}\left(d_r+\frac{1}{r}\right)(-\mathrm{i}u')-\frac{mk}{3r}v'+\left(d_{rr}+\frac{1}{r}d_r-\frac{3m^2+4k^2r^2}{3r^2}\right)w'\right], \tag{A 1d}$$

$$\rho_b\frac{\mathrm{d}T_b}{\mathrm{d}r}(-\mathrm{i}u')+(\gamma-1)P_b\left[\left(d_r+\frac{1}{r}\right)(-\mathrm{i}u')+\frac{m}{r}v'+kw'\right]+\rho(kW_b-\omega)t',$$
$$=\frac{-\mathrm{i}}{Re}\left[-2\gamma(\gamma-1)M^2(kd_rW_b(-\mathrm{i}u')-d_rW_bd_rw')+\frac{\gamma}{Pr}\left(d_{rr}+\frac{1}{r}d_r-\frac{m^2+k^2r^2}{r^2}\right)t'\right], \tag{A 1e}$$

where d_r and d_{rr} denote the r derivatives of first and second order. The pressure perturbation p' is built from ρ' and t' by the linearized ideal gas relation

$$p'=T\rho'+\rho t'. \tag{A 2}$$

Appendix B. Baroclinic effect and forced equations of motion

For clarity, we detail here the formalism only in the case of the compressible inviscid problem. However, the method is identical for the viscous equations, although additional non-homogeneous terms arise due to the presence of dissipation. Note that non-homogenous terms exist in the continuity and energy equations, but our calculations strongly suggest that their effect is negligible compared to that of the baroclinic torque.

In the presence of volumic source terms S_r, S_θ and S_z, the momentum equations can be written as

$$\partial_tu'=-W_b\partial_zu'-\frac{1}{\gamma M_\infty^2}\frac{1}{\rho_b}\partial_rp'+S_r \tag{B 1a}$$

$$\partial_tv'=-W_b\partial_zv'-\frac{1}{\gamma M_\infty^2}\frac{1}{\rho_b}\partial_\theta p'+S_\theta \tag{B 1b}$$

$$\partial_tw'=-W_b\partial_zw'-\frac{1}{\gamma M_\infty^2}\frac{1}{\rho_b}\partial_zp'+S_z. \tag{B 1c}$$

The vorticity perturbation $\boldsymbol{\Omega} = \nabla \times \boldsymbol{u}$ evolves as

$$\partial_t \Omega_r' = -W_b \left(\frac{1}{r} \partial_{\theta z}^2 w' - \partial_{zz}^2 v' \right) + \frac{1}{r} \partial_\theta S_z - \partial_z S_\theta \tag{B 2a}$$

$$\partial_t \Omega_\theta' = -W_b \left(\partial_{zz}^2 u' - \partial_{rz}^2 w' \right) + d_r W_b \partial_z w' - \frac{1}{\gamma M_\infty^2} \frac{\partial_r \rho_b}{\rho_b^2} \partial_z p' + \partial_z S_r - \partial_r S_z \tag{B 2b}$$

$$\partial_t \Omega_z' = -W_b \left(\partial_{rz}^2 v' - \frac{1}{r} \partial_{\theta z}^2 u' \right) - d_r W_b \partial_z v' + \frac{1}{\gamma M_\infty^2} \frac{\partial_r \rho_b}{\rho_b^2} \frac{1}{r} \partial_\theta p' + \partial_r S_\theta - \frac{1}{r} \partial_\theta S_r \tag{B 2c}$$

where we recognize the expression of the baroclinic torque $\boldsymbol{\Gamma} = \nabla \rho_b \times \nabla p' / \rho_b^2$.

In order to eliminate the effect of the baroclinic torque, the source terms are selected so as to satisfy

$$\frac{1}{r} \partial_\theta S_z - \partial_z S_\theta = 0, \tag{B 3a}$$

$$\partial_z S_r - \partial_r S_z = \frac{1}{\gamma M_\infty^2} \frac{\partial_r \rho_b}{\rho_b^2} \partial_z p' = \Gamma_\theta, \tag{B 3b}$$

$$\partial_r S_\theta - \frac{1}{r} \partial_\theta S_r = -\frac{1}{\gamma M_\infty^2} \frac{\partial_r \rho_b}{\rho_b^2} \frac{1}{r} \partial_\theta p' = \Gamma_z. \tag{B 3c}$$

All source terms are considered as additional variables of the generalized eigenvalue problem. The modified dispersion relation is therefore constructed from the unforced continuity and energy equations, the forced momentum equations (B 1) and the source equations (B 3).

REFERENCES

Achenbach, E. 1974 Vortex shedding from spheres. *J. Fluid Mech.* **62**, 209–221.

Batchelor, G. K. & Gill, A. E. 1962 Analysis of the stability of axisymmetric jets. *J. Fluid Mech.* **14**, 529–551.

Berger, E., Scholz, D. & Schumm, M. 1990 Coherent vortex structures in the wake of a sphere and a circular disk at rest and under forced vibrations. *J. Fluids Struct.* **4**, 231–257.

Bers, A. 1975 Linear waves and instabilities. In *Plasma Physics* (by C. De Witt, & J. Peyraud ed.), 117–215. Gordon & Breach.

Boyd, J. P. 1989 *Chebyshev and Fourier Spectral Methods*. Springer.

Briggs, R. J. 1964 *Electron Stream Interaction with Plasmas*. MIT Press.

Carroll, L. 1872 *Through the Looking-Glass: and What Alice Found There*. MacMillan.

Chomaz, J. M. 1992 Absolute and convective instability in non linear systems. *Phys. Rev. Lett.* **69**, 1931–1934.

Chomaz, J. M. 2005 Global instabilities in spatially developing flows: non-normality and nonlinearity. *Annu. Rev. Fluid. Mech.* **37**, 357–392.

Chomaz, J. M., Huerre, P. & Redekopp, L. G. 1988 Bifurcations to local and global modes in spatially developing flows. *Phys. Rev. Lett.* **60**, 25–28.

Couairon, A. & Chomaz, J.-M. 1997 Absolute and convective instabilities, front velocities and global modes in nonlinear systems. *Physica* D **108**, 236–276.

Couairon, A. & Chomaz, J.-M. 1999 Fully nonlinear global modes in slowly varying flows. *Phys. Fluids* **11** (12), 3688–3703.

Dee, G. & Langer, J. 1983 Propagating pattern selection. *Phys. Rev. Lett.* **50**, 383–386.

Deissler, R. J. 1987 The convective nature of instability in plane Poiseuille flow. *Phys. Fluids* **30** (8), 2303–2305.

Depres, D., Reijasse, P. & Dussauge, J. P. 2004 Analysis of unsteadiness in afterbody transonic flows. *AIAA J.* **42**, 2541–2550.

Drazin, P. & Reid, W. 1981 *Hydrodynamic Stability*. Cambridge University Press.

Flodrops, J. P. & Desse, J. M. 1985 Sillage d'un culot axisymétrique. Rapport 85/19. Institut de Mécanique des Fluides de Lille, France.

Fuchs, H. V., Mercker, E. & Michel, U. 1979 Large-scale coherent structures in the wake of axisymmetric bodies. *J. Fluid Mech.* **93**, 185–207.

Gallaire, F. & Chomaz, J. M. 2003 Mode selection in swirling jet experiments: a linear stability analysis. *J. Fluid Mech.* **494**, 223–253.

Gallaire, F., Ruith, M., Meiburg, E., Chomaz, J. M. & Huerre, P. 2006 Spiral vortex breakdown as a global mode. *J. Fluid Mech.* **549**, 71–80.

Hammond, D. & Redekopp, L. 1997 Global dynamics of symmetric and asymmetric wakes. *J. Fluid Mech.* **331**, 231–260.

Healey, J. J. 2005 Long-wave theory for a new convective instability with exponential growth normal to the wall. *Phil. Trans. R. Soc. Lond.* A **363**, 1119–1130.

Healey, J. J. 2006 A new convective instability of the rotating-disk boundary layer with growth normal to the disk. *J. Fluid Mech.* **560**, 279–310.

Huerre, P. & Monkewitz, P. A. 1985 Absolute and convective instabilies in free shear layers. *J. Fluid Mech.* **159**, 151–168.

Huerre, P. & Monkewitz, P. A. 1990 Local and global instabilities in spatially developing flows. *Annu. Rev. Fluid Mech.* **22**, 473–537.

Huerre, P. & Rossi, M. 1998 Hydrodynamic instabilities in open flows. In *Hydrodynamics and Nonlinear Instabilities* (C. Godrèche & P. Manneville ed.) 81–294. Cambridge University Press.

Jendoubi, S. & Strykowski, P. J. 1994 Absolute and convective instability of axisymmetric jets with external flow. *Phys. Fluids* **6** (9), 3000–3009.

Juniper, M. 2006 The effect of confinement on the stability of two-dimensional shear flows. *J. Fluid Mech.* **565**, 171–195.

Kim, H. J. & Durbin, P. A. 1988 Observations of the frequencies in a sphere wake and of drag increase by acoustic excitation. *Phys. Fluids* **31** (11), 3260–3265.

Koch, W. 1985 Local instability characteristics and frequency determination of self-excited wake flows. *J. Sound Vib.* **99**, 53–83.

Lesshafft, L. & Huerre, P. 2007 Linear impulse response in hot round jets. *Phys. Fluids* **19**(2), 024102.

Lesshafft, L., Huerre, P., Sagaut, P. & Terracol, M. 2006 Nonlinear global modes in hot jets. *J. Fluid Mech.* **554**, 393–409.

Miles, J. W. 1958 On the disturbed motion of a plane vortex sheet. *J. Fluid Mech.* **4**, 538–552.

Monkewitz, P. A. 1988 A note on vortex shedding from axisymmetric bluff bodies. *J. Fluid Mech.* **192**, 561–575.

Monkewitz, P. A. & Nguyen, L. N. 1987 Absolute instability in the near-wake of two-dimensional bluff-bodies. *J. Fluids Struct.* **1**, 165–184.

Monkewitz, P. A. & Sohn, K. D. 1988 Absolute instability in hot jets. *AIAA J.* **26**, 911–916.

Monkewitz, P. A., Bechert, D. W., Barsikow, B. & Lehmann, B. 1990 Self-excited oscillations and mixing in a heated round jet. *J. Fluid Mech.* **213**, 611–639.

Nichols, J. W., Schmid, P. J. & Riley, J. J. 2007 Self-sustained oscillations in variable-density round jets. *J. Fluid Mech.* **582**, 341–376.

Pavithran, S. & Redekopp, L. G. 1989 The absolute-convective transition in subsonic mixing layers. *Phys. Fluids* A **1** (10), 1736–1739.

Pier, B. 2002 On the frequency selection of finite-amplitude vortex shedding in the cylinder wake. *J. Fluid Mech.* **458**, 407–417.

Pier, B. & Huerre, P. 2001 Nonlinear self-sustained structures and fronts in spatially developing wake flows. *J. Fluid Mech.* **435**, 145–174.

Pier, B., Huerre, P. & Chomaz, J. M. 2001 Bifurcation to fully nonlinear synchronized structures in slowly varying media. *Physica* D **148**, 49–96.

van Saarloos, W. 1987 Dynamical velocity selection: marginal stability. *Phys. Rev. Lett.* **58**, 2571–2574.

van Saarloos, W. 2003 Front propagation into unstable states. *Phys. Rep.* **386**, 29–222.

Sato, H. & Okada, O. 1966 The stability and transition of an axisymmetric wake. *J. Fluid Mech.* **26**, 237–253.

Schlichting, H. 1978 *Boundary-Layer Theory*, 7th edn. McGraw–Hill.

Schmid, P. J. & Henningson, D. S. 2001 *Stability and Transition in Shear Flows*. Springer.

Sevilla, A. & Martínez-Bazàn, C. 2004 Vortex shedding in high Reynolds number axisymmetric bluff-body wakes: local linear instability and global bleed control. *Phys. Fluids* **16** (9), 3460–3469.

Soteriou, M. C. & Ghoniem, A. F. 1995 Effects of the free-stream density ratio on free and forced spatially developing shear layers. *Phys. Fluids* **7** (8), 2036–2051.

Tobias, S. M., Proctor, M. R. E. & Knobloch, E. 1997 The role of absolute instability in the solar dynamo. *Astron. Astrophys.* **318**, 55–58.

Tobias, S. M., Proctor, M. R. E. & Knobloch, E. 1998 Convective and absolute instabilities of fluid flows in finite geometry. *Physica* D **113**, 4–72.

Yu, M. H. & Monkewitz, P. A. 1990 The effect of non uniform density on the absolute instability of two-dimensional inertial jets and wakes. *Phys. Fluids* A **2** (7), 1175–1181.